Extended hot dust emission around the earliest massive quiescent galaxy

Zhiyuan Ji[1*], Christina C. Williams[2,1], George H. Rieke[1],
Jianwei Lyu[1], Stacey Alberts[1], Fengwu Sun[3], Jakob M. Helton[1],
Marcia Rieke[1], Irene Shivaei[4], Francesco D'Eugenio[5,6],
Sandro Tacchella[5,6], Brant Robertson[7], Yongda Zhu[1],
Roberto Maiolino[5,6,8], Andrew J. Bunker[9], Yang Sun[1],
Christopher N. A. Willmer[1]

[1*]Department of Astronomy, University of Arizona, 933 N. Cherry
Avenue, Tucson, 85721, Arizona, USA.
[2]NSF's National Optical-Infrared Astronomy Research Laboratory, 950
N. Cherry Avenue, Tucson, 85719, Arizona, USA.
[3]Center for Astrophysics, Harvard & Smithsonian, 60 Garden Street,
Cambridge, 02138, Massachusetts, USA.
[4]Centro de Astrobiología (CAB), CSIC-INTA, Carretera de Ajalvir km
4, Torrejón de Ardoz, Madrid, 28850, Spain.
[5]Kavli Institute for Cosmology, University of Cambridge, Madingley
Road, Cambridge, CB3 0HA, UK.
[6]Cavendish Laboratory, University of Cambridge, 19 JJ Thomson
Avenue, Cambridge, CB3 0HE, UK.
[7]Department of Astronomy and Astrophysics, University of California,
Santa Cruz, 1156 High Street, Santa Cruz, 95064, California, USA.
[8]Department of Physics and Astronomy, University College London,
Gower Street, London, WC1E 6BT, UK.
[9]Department of Physics, University of Oxford, Denys Wilkinson
Building, Keble Road, Oxford, OX1 3RH, UK.

*Corresponding author(s). E-mail(s): zhiyuanji@arizona.edu;

arXiv:2409.17233v1 [astro-ph.GA] 25 Sep 2024

1

Abstract

A major unsolved problem in galaxy evolution is the early appearance of massive quiescent galaxies that no longer actively form stars only $\sim$1 billion years after the Big Bang. Their high stellar masses and extremely compact structure[1] indicate that they formed through rapid bursts of star formation[2,3] between redshift $\boldsymbol{z \sim 6 - 11}$[4,5,6,7]. Theoretical models of galaxy evolution cannot explain their high number density, rapid growth and truncation of star formation at such early times[8,9], which likely requires extreme feedback to destroy the cold interstellar medium (the fuel for star formation). We report the discovery of a significant reservoir of hot dust in one of the most distant known examples at $\boldsymbol{z = 4.658}$, GS-9209[10]. The dust was identified using JWST's Mid-Infrared Instrument (MIRI), whose unprecedented sensitivity and high spatial resolution, for the first time, firmly show that this dust is significantly more extended than the stars by $\gtrsim \boldsymbol{3}$ times. We find that the dust has preferentially been evacuated or diluted in the galaxy center. Our analysis finds that the extended hot dust emission is consistent with recent heating by a younger and more spatially extended generation of star formation. This reveals that the earliest quiescent galaxies did not form in a single rapid burst; instead, similar to galaxy growth at later times, the center formed first with star formation continuing in an extended envelope. The growth of this galaxy is truncating from the inside out, consistent with central gas depletion from early AGN feedback.

The galaxy presented here, GS-9209, is so far one of the earliest known massive quiescent galaxies in the Universe with a spectroscopically confirmed redshift of $z = 4.658$[10]. JWST's NIRCam observations[1] revealed that the rest-optical/NIR half-light radius of GS-9209 is only $r_e \sim 200$ pc, which corresponds to a stellar mass surface density of $\sim 10^{11} M_\odot/\mathrm{kpc}^2$ approaching the maximum allowed density set by stellar feedback[11]. The formation of such an extremely compact stellar morphology, and its connection to the very early truncation of star formation pose major challenges to models of massive galaxy formation in the early Universe.

In December 2022, we obtained 8-band imaging of GS-9209 at observed wavelengths $\lambda_{\mathrm{obs}} \sim 5 - 30\mu m$ with the Mid-Infrared Instrument[12] (MIRI) of the James Webb Space Telescope[13] (JWST) through the SMILES program[14,15]. With the MIRI observations, for the first time in a massive quiescent galaxy at this redshift, we are able to constrain emission red-ward of the stellar bump at rest-frame $\lambda_{\mathrm{rest}} = 1.6\mu m$ [*]. This allows us to put new constraints that were entirely missed by previous observations – the presence of dust emission from GS-9209.

The MIRI images of GS-9209 are shown in Fig. 1, where the λ_{rest} range probed by each band is indicated. At $\lambda_{\mathrm{obs}} \sim 6 - 10\mu m$ which corresponds to $\lambda_{\mathrm{rest}} \sim 1 - 2\mu m$, MIRI images show a very compact morphology, suggesting a nucleated, high-density stellar distribution of GS-9209, which is fully consistent with the studies using shorter wavelength NIRCam observations[10,1].

---

[*]Because H^- ion has the minimal opacity at this wavelength, the emission of cool stars shows a maximum/bump in galaxies' SEDs.
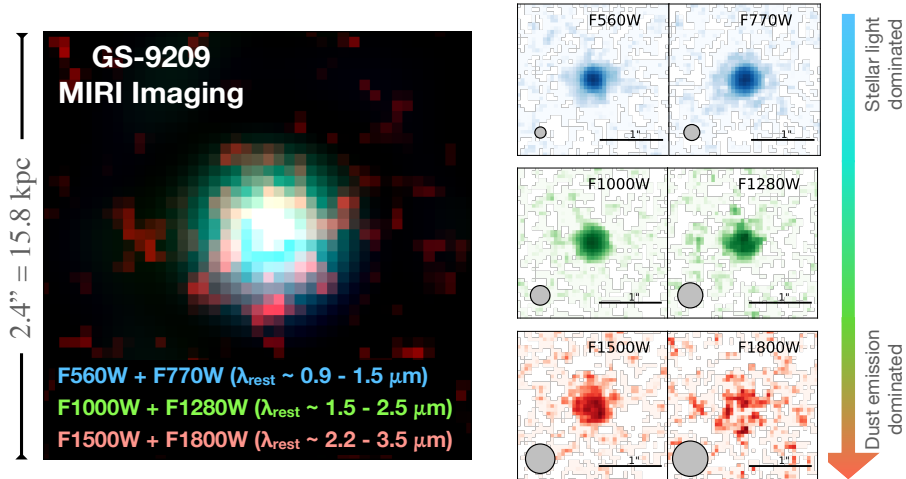
Fig. 1 MIRI imaging of GS-9209. Images shown here are F560W, F770W, F1000W, F1280W, F1500W, F1800W bands that cover $\lambda_{\rm obs} \sim 5.6$, 7.7, 10.0, 12.8, 15.0 and 18.0 μm, respectively. On the left we show the pseudo-RGB image made of the PSF-matched MIRI images. On the right we show the images, in the nominal angular resolution, of individual MIRI bands. From F560W to F1800W, the MIRI imaging samples the spectral range from $\lambda_{\rm rest} \sim 1\mu m$ to $\lambda_{\rm rest} > 3\mu m$, where the contribution from the dust emission becomes increasingly important relative to the starlight.

Remarkably, moving towards longer wavelengths of $\lambda_{\rm obs} > 10\mu m$, MIRI imaging starts to show more extended emission from GS-9209 than appears at shorter wavelengths. Using source injection simulations, we quantitatively compare GS-9209's light distributions at $\lambda_{\rm obs} > 10\mu m$ to its starlight probed by F770W (see Methods). As Fig. 2 shows, the F1500W ($\lambda_{\rm rest} \sim 2.7\mu m$) starts to significantly depart from the stellar profile, a tendency that becomes clearer in both the image and radial profile at F1800W ($\lambda_{\rm rest} \sim 3.2\mu m$). The confidence level that the light profiles are significantly different is $p > 99.99\%$. This difference in light profile is twofold. First, relative to the starlight, F1500W and F1800W images show more extended emission at $0".4 < r < 0".6$ from the center, with a confidence level of $p = 99.06\%$ for F1500W and 99.76% for F1800W. Second, near the center ($r \sim 0".15$) of GS-9209, there appears a flux deficit in the F1800W image, with a confidence level of $p = 98.7\%$. As we show in Methods, a similar central flux deficit is also observed in the F2100W image ($\lambda_{\rm rest} \sim 4\mu m$) despite the tentative (S/N ~ 4) detection of GS-9209 in it.

We further study the MIRI light profiles of GS-9209 through two-dimensional parametric light profile fitting. To begin, we assume a single Sérsic profile [16] and simultaneously model the MIRI images from F560W to F1800W (see Methods). As Fig. 3 shows, r_e increases towards longer-wavelength MIRI bands. The r_e (from the single Sérsic fitting) of F1800W is ≈ 450 pc which is $\sim 2 - 3$ times larger than GS-9209's starlight. Motivated by the analysis of the Spectral Energy Distribution (SED) detailed below, where we find the observed MIRI fluxes at $\lambda_{\rm rest} > 2.5\mu m$ come from both AGN

3

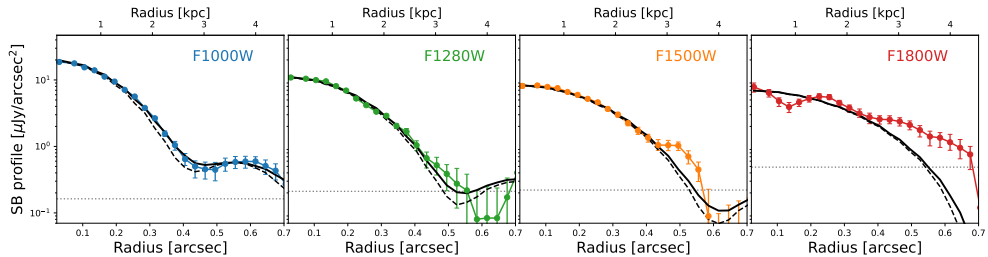**Fig. 2 Radial surface brightness profiles of GS-9209 in JWST/MIRI bands at $\lambda_{\rm obs} > 10\mu m$.** In each panel, the observed surface brightness profile is shown as colored points with error bars. The horizontal grey dotted line marks the 3σ detection limit. The black solid line and shaded region show the median and 1σ of the expected surface brightness profile from our source injection simulations, assuming the galaxy's total light distribution at $\lambda_{\rm obs} > 10\mu m$ were the same as its stellar light. Similarly, the black dashed line shows the expected surface brightness profile for a point source in MIRI. At $\lambda_{\rm obs} > 15\mu m$, corresponding to $\lambda_{\rm rest} \gtrsim 2.5\mu m$, the light distribution (hot dust emission) of GS-9209 is more extended than its stellar light.
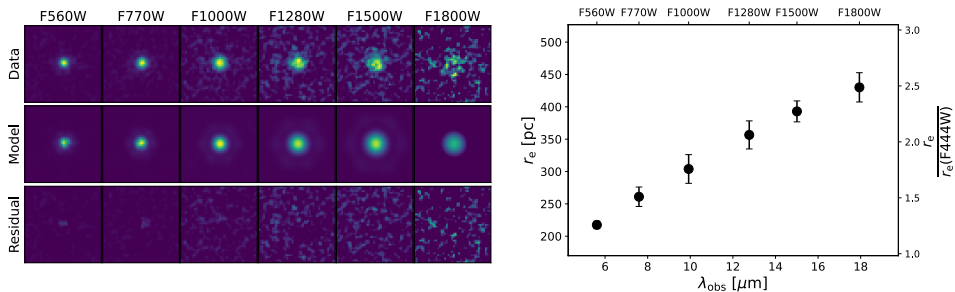

Fig. 3 Two-dimensional light profile fitting of GS-9209. We model the light profile of each one of the MIRI images with a single Sérsic profile. On the left, we show the comparison between data and best-fit models. On the right, the variation of $r_{\rm e}$ as a function of wavelength is plotted. The half-light size of the hot dust emission of GS-9209 is significantly more extended than its starlight.

torus and dust emission of diffuse ISM, we also fit the F1500W and F1800W images using an alternative two-component model, namely a PSF plus a Sérsic profile. As expected, this two-component fitting returns a larger $r_{\rm e}$ of ≈ 2 kpc, almost 10 times of GS-9209's starlight. In Methods, we further test our results by assuming other different light profiles. In all cases the same conclusion is reached that the light distribution of GS-9209 at $\lambda_{\rm rest} > 2.5\mu m$ is significantly more extended than its starlight, in excellent agreement with our source injection simulations mentioned before. Depending on the assumed light profiles, we estimate the size of GS-9209 at $\lambda_{\rm rest} > 2.5\mu m$ to be larger than its starlight by at least $\sim 2 - 3$ times, and up to 10 times.

One key revelation from multiple decades of Hubble Space Telescope (HST)[17,18,19,20] and now JWST/NIRCam[1,21] observations was that the majority of massive quiescent galaxies at $z > 1.5$ have extremely compact stellar morphology.
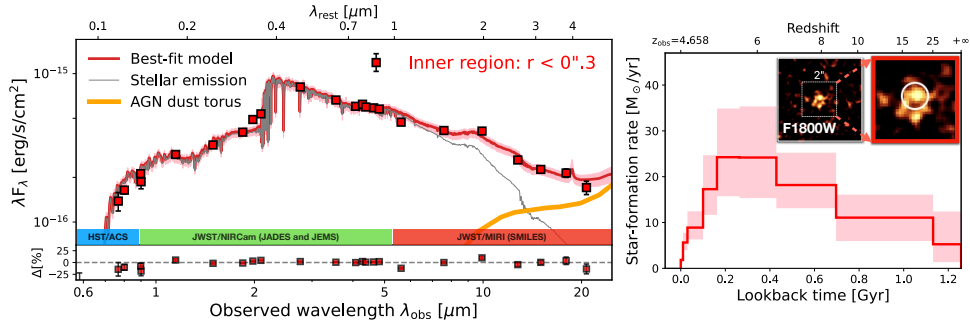
Fig. 4 Spectral energy distribution of the inner region ($r < 0".3$) of GS-9209. The left panel shows the comparison between data (squares with error bars) and the best-fit SED model, where the bottom inset shows the relative difference, i.e. (Data − Model)/Data. MIRI provides key constraints on the emission red-ward the rest-$1.6\mu m$ stellar bump, where the shape of GS-9209's inner SED is inconsistent with the emission from stars alone (grey curve). Hot dust emission from AGN torus (orange) is required to reproduce the MIRI observations. The right panel shows the reconstructed nonparametric star-formation history of the inner region, where solid line and shaded area mark the best-fit and 1σ uncertainty, respectively. The inset shows the zoomed-in view of GS-9209's F1800W image, with an $r = 0".3$ circular aperture overplotted.

Moreover, earlier studies found that these galaxies also seem to have rather simple (HST) light profiles[22,23] that can be well described by a single morphological component. Yet, our MIRI observations immediately reveal that the structure of GS-9209 is much more complex than we previously thought about typical high-redshift compact quiescent galaxies: Apart from an extremely compact stellar core at the center, GS-9209, one of the earliest known massive quiescent galaxies, has more extended morphological components, and evidence for substructures (e.g. a near-center flux deficit), at $\lambda_{rest} \gtrsim 2.5\mu m$.

To investigate the physical origin of the MIRI fluxes, we model the SED of GS-9209 (see Methods) using the combined photometry from the legacy HST/ACS imaging[24], the NIRCam imaging from the JADES[25] and JEMS[26] programs, and our new MIRI imaging. Using the integrated photometry (i.e. total observed flux), we obtain quantitatively consistent measures of the stellar-population properties of GS-9209 with those from the SED fitting of Carnall et al.[10] using NIRSpec spectrum (see Methods).

Crucially, the immense gain of JWST over previous mid-infrared telescopes – about two orders of magnitude in sensitivity and an order of magnitude in angular resolution compared to Spitzer[14] – now allows us to perform spatially resolved SED analysis to investigate the detailed internal structure of the earliest massive quiescent galaxies at mid-infrared wavelengths, a knowledge of quiescent galaxies that was totally uncharted beyond the local Universe before JWST.

We present the fiducial SED fitting results of GS-9209's inner region enclosed by an $r = 0".3$ circular aperture in Fig. 4, and of GS-9209's outer region enclosed by an $r = 0".3 - 0".7$ circular annulus aperture in Fig. 5.

GS-9209's outer region is younger and more dust-attenuated than its inner region. For the inner region, the best-fit model has little instantaneous star-formation activity
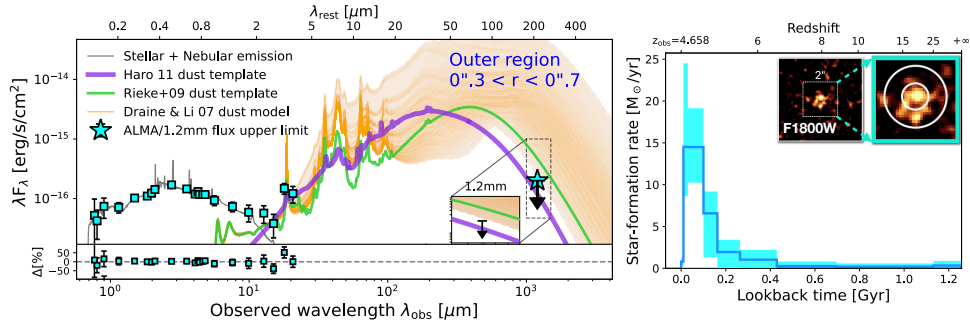
Fig. 5 Spectral energy distribution of the outer region (0".3 < r < 0".7) **of GS-9209.** Similar to Fig. 4, the left and right panels show the best-fit SED model and reconstructed star formation history. Hot dust emission of diffuse ISM is required to reproduce the observed MIRI fluxes. Different dust templates extensively used in the literature are assumed, including Draine and Li [27], Rieke et al. [28], and the one of Haro 11 [29]. The ALMA non-detection (based on archival data) of GS-9209 suggests that the dust emission of GS-9209 is more consistent with that of Haro 11.

with a specific star formation rate of $\log\left(\mathrm{sSFR/yr^{-1}}\right) = -10.0^{+0.2}_{-0.4}$, a mass-weighted stellar age of $t_{\mathrm{age}} = 500 \pm 100$ Myr or a formation redshift of $z_{\mathrm{form}} = 6.8 \pm 0.5$, and low dust attenuation with $\mathrm{E(B-V)} = 0.16 \pm 0.01$ mag. Comparatively, the outer region has younger stellar populations with a larger $\log\left(\mathrm{sSFR/yr^{-1}}\right) = -9.5^{+0.2}_{-0.2}$ and smaller $t_{\mathrm{age}} = 160 \pm 60$ Myr or $z_{\mathrm{form}} = 5.1 \pm 0.1$, and higher dust attenuation with $\mathrm{E(B-V)} = 0.47 \pm 0.08$ mag. In Methods, we test our results by altering the default SED assumptions (star-formation history, metallicity etc.). We show that our conclusions are insensitive to the assumptions made in the fiducial SED fitting.

The spatial difference in stellar populations immediately shows that the formation of GS-9209 did not occur in a single episode. Instead, its formation is in an inside-out manner, which is similar to star-forming galaxies, but with a much higher efficiency since its major star formation has already halted merely $\lesssim 1$ Gyr after the Big Bang.

Starting from $\lambda_{\mathrm{obs}} \sim 10\mu m$ or $\lambda_{\mathrm{rest}} \sim 2.5\mu m$, the SED of GS-9209 cannot be explained by purely stellar light alone. The dust emission is required to reproduce the observed MIRI fluxes, for both the inner and outer regions.

For the inner region, SED analysis suggests that the emission at $\lambda_{\mathrm{rest}} \sim 2.5\mu m$ is dominated by AGN torus, a conclusion that is independent of assumed AGN templates (see Methods). We stress that the reprocessed emission of dust associated with diffuse ISM is also included to the SED modeling. Yet, the fitting still finds that the mid-infrared SED of the inner region is consistent with being dominated by AGN, suggesting the lack of significant amount of dust associated with diffuse ISM at the center of GS-9209 (Fig. 4). It is also worth mentioning that, SED fitting using only the shorter wavelength (no MIRI) photometry was ambiguous about the AGN presence in GS-9209 [1], although the presence of a faint one is demonstrated by the broad Hα line [10]. The detection in our full set of photometry, and the consistency of our SED-inferred AGN luminosity and that derived from NIRSpec spectroscopy (see Methods) show the power of MIRI in identifying and characterizing AGNs just with photometry.

6

For the outer region of GS-9209, we find that the $\lambda_{\mathrm{rest}} > 2.5\mu m$ emission is observed on kpc-scales, exceedingly larger than the typical (sub-)pc scale of the AGN-heated torus emission at these wavelengths[30,31]. This suggests that the dust emission has to be associated with diffuse ISM. Regardless of assumed dust templates, however, if we adopt the energy balance criterion where all starlight attenuated by the dust is re-emitted in infrared, we find that the MIRI fluxes at $\lambda_{\mathrm{rest}} \sim 2.5\mu m$ is not well-modeled (see Methods). In fact, earlier studies have questioned the use of the energy balance assumption especially when the UV and IR emission of galaxies is offset from one another[32]. Given the significant difference in GS-9209's stellar and dust morphologies revealed by our MIRI imaging, the ineffectiveness of the energy balance is arguably expected for GS-9209.

Without the assumption of energy balance, as Fig 5 shows, different dust emission templates are all able to fit the HST-to-MIRI photometry reasonably well. The non-detection of GS-9209 from archival ALMA observations[33] provides additional, critical constraints on its dust properties. We derive an upper limit at observed 1.2 mm (or $\lambda_{\mathrm{rest}} \sim 210\mu m$) of 80 μJy with forced photometry following Williams et al.[34]. This limit is inconsistent with typical dust models assumed for massive star-forming galaxies[27,28]. Instead, it is broadly consistent with the dust emission template of Haro 11, a starbursting dwarf galaxy in the local Universe whose IR SED – relative to typical star-forming galaxies – features a higher dust temperature ($\sim$47 K) and an excess of near-to mid-IR continuum emission likely from additional even warmer dust[31]. GS-9209 and Haro 11 share two major similarities, namely a low metallicity and very compact morphology, which indeed have been shown to lead to a warmer/bluer IR SED similar to that of Haro 11[35]. Future spectroscopy at mid-to-far infrared wavelengths is required to further quantify the dust properties in such systems.

Combining together our morphological and SED analysis, we conclude that there is a significant dust reservoir in GS-9209. The hot dust emission has two origins. At the center, the emission is dominated by AGN torus. In the outskirts of GS-9209 where its stellar population is younger than the inner region, the extended $\lambda_{\mathrm{rest}} > 2.5\mu m$ emission is associated with the hot dust of diffuse ISM, mostly likely powered by rest-frame UV/optical starlight absorbed by the dust and re-emitted in IR.

The discovery that the first massive quiescent galaxies like GS-9209 form and quench from the inside out now enables new empirical constraints on their formation pathways. The structure of GS-9209, namely a compact older stellar core surrounded by a younger stellar and dust envelope, is very similar to the hallmark prediction for the gas-rich processes associated with galaxy formation[36]. Physically, the formation of the extremely dense stellar core requires highly dissipative gas accretion[37]. The buildup of the core in turn will deepen the gravitational potential well, making the later, continuous accretion of gas and satellite mergers settle into orbits surrounding the older central core. Interestingly, hydrodynamical simulations with adequate resolution for the modeling of relevant gaseous astrophysics predict that continuous gas accretion (while star-formation at the center is effectively halted) should form a extended, ring structure in massive galaxies at a physical scale of $r \gtrsim 3\,r_{\mathrm{e}}^{\mathrm{star}}$ at $z < 4$[38,39,40], in

quantitative agreement with the scale where the extended hot dust emission of GS-9209 is observed. Thus, the gas-rich processes found at $z < 4$ may plausibly extend to higher redshifts for the formation of this earlier generation of massive galaxies[1].

Near the center, the likely flux deficit at $\lambda_{\rm rest} > 2.5\mu$m (Fig. 1, 2), and the lack of evidence of the presence of dust associated with diffuse ISM (Fig. 4) imply central gas depletion as a direct cause of the inside-out quenching of GS-9209. A natural consequence of highly dissipative gas accretion is also the faster, more efficient growth of supermassive black holes[41,42]. The impact of this is that AGN feedback may become energetic enough to impact the host galaxy on faster timescales, helping to heat up and even expel gas. GS-9209 indeed hosts an AGN, which indicates that the AGN feedback might be the cause of the vacated dust/gas near the center.

We finally discuss our MIRI discovery of the extended hot dust emission from GS-9209 in the cosmological context. Numerous studies have now noted that state-of-the-art cosmological simulations fail to quantitatively reproduce the observed number density of massive quiescent galaxies that form at $z > 3$[43,44,8,9]. A common attribute among these simulations is that the AGN feedback, in particular the black hole seeding time and the time at which kinetic quasar-mode feedback becomes influential, does not occur early enough in cosmic time[45,46,47]. This has been identified as a likely cause why quenching in simulations occurs too late. The discovery by JWST of abundant supermassive black holes earlier and more massive than expected[48,49] further corroborates this evidence that AGN feedback is more prevalent and impacts their host galaxies earlier than previously thought. If GS-9209 is a good representative of the general population of earliest massive quiescent galaxies, our MIRI observations provide strong evidence that the gas-rich dissipative processes and AGN feedback play a critical role in the formation and quenching of the earliest quiescent galaxies discovered by JWST. Simulations of sufficiently massive halos at $z > 5$ with the resolution to adequately model gas-rich galaxy growth do not currently exist, but this advance is needed to determine whether the detailed physical properties of galaxies like GS-9209, such as the multi-wavelength structure, are in tension with cosmological expectations.

With its revolutionary capabilities, particularly the unprecedented angular resolution, JWST's MIRI now opens a new window of studying high-redshift, freshly quenched galaxies through the spatial distribution of dust emission, promising powerful constraints on the physical mechanisms responsible for the cessation of star formation in the earliest massive quiescent galaxies.

Methods

1 Cosmology model and definitions

Throughout this study, we adopt the ΛCDM cosmology with $H_0 = 70$ km s^{-1} Mpc^{-1}, $\Omega_{\rm m} = 0.3$ and $\Omega_\Lambda = 0.7$. All magnitudes are presented in the AB system.

2 NIRCam and MIRI imaging data reduction

GS-9209 appears in the medium-depth portion of the JADES program in GOODS-South[25,50], where we have obtained JWST/NIRCam imaging in 8 bands, F090W, F115W, F150W, F200W, F277W, F356W, F410M and F444W. Additional 5 medium-band NIRCam images, i.e. F182M, F210M, F430M, F460M and F480M, were obtained by the JEMS program[26]. We also include public, shallower F182M, F210M and F444W imaging from the FRESCO survey[51] to further improve the depth of those images. We reduce all NIRCam imaging observations using the pipeline developed by JADES, the details of which have been presented in Rieke et al.[52]. In brief, we process the raw images using the JWST Calibration Pipeline with the following custom corrections. During Stage 1 of the JWST pipeline, we mask and correct for the "snowballs"[†] cosmic-ray artefacts. During Stage 2 of the JWST pipeline, we remove the $1/f$ noise and subtract 2D background from the images, and also correct the "wisp" scattered light features. Afterwards, we tie the astrometry of individual exposures of a given visit to the World Coordinate System (WCS) of a reference catalog constructed from HST/WFC3 F160W mosaics in GOODS-South with astrometry tied to Gaia-EDR3[53]. Before combining visit-level images to create the final mosaic, we manually inspect all individual exposures containing GS-9209. We remove two out of six F090W exposures from our analysis as the "snowballs" effect is seen in very close proximity (< 2") of GS-9209 and significantly affects the surrounding sky.

GS-9209 also appears in the JWST/MIRI program, SMILES[14,15], where we have obtained MIRI images in 8 bands, F560W, F770W, F1000W, F1280W, F1500W, F1800W, F2100W and F2550W. We reduce MIRI imaging observations using the nominal JWST Pipeline with the latest JWST Calibration Reference System. We make custom modifications for sky subtraction which has been described in detail in Alberts et al.[15]. In brief, to better correct for the large spatial gradient of sky background in our data and remove substructures including tree-ring shaped features along the columns and rows of the MIRI detector, for each one of the cal files (i.e., the products of the CALWEBB_IMAGE2 in JWST Pipeline), we adopt an iterative process to (1) progressively mask sources, (2) median filter out large-scale sky gradients and striping features along detector columns and rows and (3) construct a super background by median combining and scaling all those filtered cal files. Finally, we subtract from each cal file the super background, after which we do an additional median subtraction using a 256×256 pixel^2 box to remove remaining background variations, which are mainly caused by cosmic ray showers. We tie the astrometry of MIRI mosaics to be the same as JADES.

Current imaging depth of MIRI/F2100W from SMILES results in a signal-to-noise ratio S/N ~ 4 detection of GS-9209 (Fig. 6). For the reddest MIRI band F2550W, GS-9209 is not detected (S/N < 1) which however is expected based on the detection limit of SMILES. The results of these two band MIRI images are not included to the main text.

[†]https://jwst-docs.stsci.edu/jwst-near-infrared-camera/nircam-instrument-features-and-caveats/nircam-claws-and-wisps
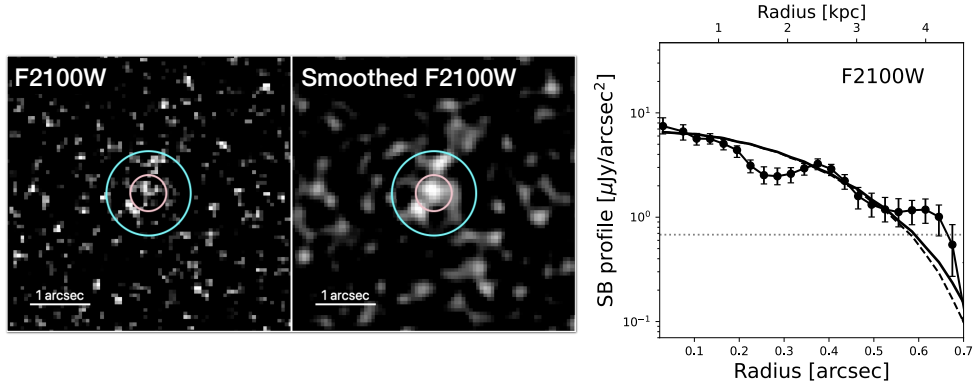
Fig. 6 MIRI/F2100W observations of GS-9209. The left panel shows the original F2100W image. The middle panel shows the F2100W image smoothed with a $\sigma = 1$ pixel Gaussian kernel. The pink and cyan circles have a radius of 0".3 and 0".7, respectively. The right panel shows the result of source injection simulations, similar to those shown in Fig. 2.

3 Analysis of MIRI light profiles

3.1 Source injection simulations

The main goal of this analysis is to compare observed light distributions of GS-9209 at $\lambda_{\mathrm{obs}} > 10\mu m$ with its stellar light distribution. A common method is through parametric morphology modeling, e.g. Sérsic fitting, to compare the fitted parameters at different wavelengths. We stress, however, that the spatial distribution of hot dust emission in high-redshift quiescent galaxies is largely unknown at present. Thus, the mismatch between the assumed parametric light profile and the intrinsic distribution of hot dust emission can make such comparison fraught with systematic errors. To mitigate this issue, we decide to make the comparison through a purely empirical method – source injection simulations.

The idea is to inject artificial sources with the same light distribution of GS-9209's starlight (F770W) into empty regions of MIRI images at $> 10\mu m$, and then to measure surface brightness profiles of these injected sources with the same procedure used for GS-9209. If the light distributions of GS-9209 at $\lambda_{\mathrm{obs}} > 10\mu m$ differ from its starlight distribution, then we expect the observed surface brightness profiles of GS-9209 at $\lambda_{\mathrm{obs}} > 10\mu m$ to be different from the recovered profiles of the realizations (i.e. injected artificial sources).

For source injections, we first create artificial galaxy images mimicking the stellar light distribution of GS-9209. The typical light distribution of $z > 3$ quiescent galaxies at rest-frame NIR remains largely unknown, but can be complex[1]. Thus, instead of assuming a parametric, likely over-simplified profile of GS-9209's starlight distribution, we directly use its MIRI/F770W image to generate synthetic images at longer wavelengths. The choice of F770W is because (1) GS-9209 is detected in F770W at

10

high S/N (= 72, using a $r = 0.25$" circular aperture), (2) AGN contribution is negligible at F770W based on multiple different analyses of GS-9209's SED, and (3) at GS-9209's redshift $z = 4.658$, F770W probes $\lambda_{\mathrm{rest}} = 1.0 \sim 1.7 \mu m$ – covering the $1.6 \mu m$ stellar bump – which is a very sensitive to (and arguably the best available probe of) the spatial distribution of stars in GS-9209.

We PSF-match the F770W image to the MIRI bands at $\lambda_{\mathrm{obs}} > 10 \mu m$. We rescale the PSF-matched F770W image of GS-9209 such that the flux within a $r = 0.2$" circular aperture is matched to that observed at longer wavelengths. We then use the MIRI segmentation map to mask out all detected sources, and inject the rescaled synthetic images to the $1' \times 2'$ ($\sim$ the field of view of MIRI imaging) region centered around GS-9209. We randomly inject these images 10^4 times, and each time we also resample the synthetic image with the Poisson noise calculated using the corresponding exposure time maps of our MIRI observations. Finally, we measure the surface brightness profiles of the injected artificial sources. The median and 1σ range of the surface brightness profiles of the 10^4 realizations are shown as black solid line and shaded region in Fig. 2. In addition to injecting artificial sources with the observed F770W light profile, we also run another set of simulations to inject entirely unresolved point sources. In Fig. 2, the median surface brightness profiles of the injected artificial point sources are shown as black dashed line.

Before moving forward, we stress that, in contrast to simply comparing the PSF-matched F770W image of GS-9209 to its images at longer wavelengths, source injection simulations take into account the realistic noise behaviors of the MIRI observations, allowing us to have a robust estimate on the significance of the difference in light profiles between the stellar light and hot dust emission of GS-9209.

We first test the null hypothesis that the observed light distributions of GS-9209 at $\lambda_{\mathrm{obs}} > 10 \mu m$ are similarly compact to its stellar light distribution. Out of 10^4 realizations, only in 94 and 24 cases is the surface brightness profile of injected artificial sources as bright or brighter than that observed in F1500W and F1800W within a $0".4 < r < 0".7$ annulus aperture. We thus reject the null hypothesis with a p-value of 99.06% and 99.76% for the F1500W and F1800W images, respectively. This shows that the observed MIRI light distributions of GS-9209 at $\lambda_{\mathrm{rest}} > 2.5 \mu m$ (hot dust emission) are more extended than its stellar light. We note that, despite GS-9209 only being detected with a moderate significance in MIRI/F2100W, source injection simulations were still preformed for F2100W and the results are shown in the right panel of Fig. 6. Owing to the relatively low S/N, the observed F2100W light profile at $0".4 < r < 0".7$ is within 1σ range of the source injection simulations, although the observed one is above the median surface brightness profile measured from the simulations, i.e. in line with the results of F1500W and F1800W.

Relative to the stellar light distribution, there appears to be a flux deficit near the center ($r \sim 0".15$) of GS-9209 in its F1800W image (Fig. 1 and 2). Such an angular scale is smaller than the resolution of MIRI/F1800W imaging (FWHM/2 $\sim 0".25$), making it very difficult, if at all possible, to quantify precisely the physical scale over which the flux deficit is present. Nonetheless, with source injection simulations, we can at least test the null hypothesis that this deficit is a result of noise fluctuations. Out of 10^4 realizations, the surface brightness profiles of 130 injected artificial sources are as faint or fainter than that observed in F1800W within a $0".12 < r < 0".18$ annulus

11

aperture. We thus reject the null hypothesis with a p-value of 98.7%. We note that, at a similar angular scale (0".15 $< r <$ 0".3), a flux deficit is also observed in the F2100W image (Fig. 6). We thus believe this deficit to be a real feature of GS-9209's hot dust emission.

Finally, among F1800W surface brightness profiles of the 10^4 injected artificial sources, none of them has both the near-center flux deficit at $r \sim$ 0".15 and more extended emission at 0".4 $< r <$ 0".7. Thus, the stellar and hot dust distributions of GS-9209 are different at a significance level of $> 99.99\%$. We stress again that we intend to make the source injection simulations as empirical as possible such that our conclusions have the least dependence, if at all, on the assumptions made. We conclude that the hot dust distribution of GS-9209 differs significantly from its starlight.

3.2 Parametric light-profile fitting

For high-redshift quiescent galaxies, we reiterate that the spatial distribution of hot dust emission is unknown. Nonetheless, a meaningful estimate of the difference between the stellar and hot dust distributions is still very important, as this will enable quantitative comparisons between the MIRI observations and predictions from hydrodynamical simulations. In what follows, we thus use a few commonly assumed parametric light profiles to model the MIRI images, in an attempt to quantify the difference in size between the stellar and hot dust emission of GS-9209.

The analysis is done by performing PSF-convolved fitting of the 2D light distributions from F560W to F1800W. We use the software GALFITM [54,55] that is built upon GALFIT3 [56] but also allows simultaneously modeling multi-band images. For PSF models of MIRI images at $\lambda_{\rm obs} > 10\mu m$, i.e. from F1000W to F1800W, there is a very limited number of MIR-bright point sources in the SMILES footprint, leading to noisy outskirts of the empirical PSF models. To mitigate this, instead of using the empirical PSFs, we build model PSFs at $\lambda_{\rm obs} > 10\mu m$ following the strategy used for the NIRCam imaging of JADES [57]. In short, we first inject the WEBBPSF [58] models into the individual stage-2 images, and then mosaic them following the same stage-3 data reduction of SMILES. The PSF models are then constructed from these PSF-mosaics. The empirical and model PSFs agree with each other very well at the center, but model PSFs have a much more stable behavior at the outskirts. For F560W and F770W, we do not use model PSFs, because the cross-shaped artifact (a.k.a. cruciform), an extended artifact caused by internal reflection in the F560W and F770W detectors [59], is not well captured in current WEBBPSF modeling. Instead, for F560W and F770W we use the empirical PSF models built upon observed point sources in SMILES following the method of Anderson and Bedin [60].

To begin, we first assume a single Sérsic profile for each one of the MIRI images. By default, because the S/N of the detections decrease with wavelength, we simultaneously model all MIRI images such that the fit uses the information of all the available data while allowing parameters to vary as a smooth function of wavelength. Such an approach has been demonstrated to provide more stable and accurate multi-wavelength morphological parameters than modeling images of different bands independently, particularly when some images have low-to-moderate S/N [54,61,62,55]. During the fitting, we fix the sky background to the 3σ-clipped median pixel value

of a 5" × 5" cutout after masking all detected sources using the segmentation map. We fit the center, axis ratio and position angle as free parameters, but assume they do not vary with wavelength. We fit the Sérsic index n and allow it to change freely with wavelength. The main parameter of interest, the effective radius r_e, is assumed to vary with wavelength following a second order Chebyshev polynomial, following recent studies[62]. To derive the uncertainties of the fitted parameters, we use the error flux extension of the MIRI images to Monte Carlo resample the image pixel values, and then run GALFITM. We repeat the procedure 1000 times, and use the standard deviation as the parameter uncertainties. The fitting results are shown in Fig. 3. We obtain $r_e = 217 \pm 10$ pc in F560W and $r_e = 261 \pm 17$ pc in F770W, in good agreement with the size measured from the NIRCam observations within the uncertainty[10,1]. For F1800W, we obtain $r_e = 430 \pm 27$ pc.

We test the single Sérsic fitting results above by modeling each one of the MIRI images independently, namely that, except fixing the centroid, all other parameters, axis ratio, position angle, Sérsic index n and r_e are allowed to vary freely with wavelength. We obtain $r_e = 216 \pm 12$, 225 ± 17 and 461 ± 49 pc in F560W, F770W and F1800W, respectively. We also test our results by (1) fitting the sky background as a free parameter and (2) using empirical PSFs (though low S/N at outskirts) at $\lambda_{\rm obs} > 10\mu m$. We do not see any substantial changes in our results. Therefore, our parametric light-profile fitting reaches to the same conclusion as our source injection simulations: The light distribution of GS-9209 at $\lambda_{\rm rest} > 3\mu m$ is more extended than its stellar light. Assuming a single Sérsic profile, the size of hot dust emission of GS-9209 is $\gtrsim 3$ times larger than its stellar light.

The quantitative difference in size between the stellar and hot dust emission depends on the parametric light profile assumed for the modeling. The presence of AGN in GS-9209, which is revealed by both broad Hα emission[10] and our SED fitting with MIRI, motivates the fit to the MIRI images using an alternative two-component model, a PSF component to account for the AGN, plus a Sérsic component to account for the host galaxy. During this modeling, each one of the MIRI images is fitted independently. From F560W to F1280W, the PSF+Sérsic fitting returns essentially the same results as the single Sérsic fitting: flux contribution from the PSF component is $< 10\%$. The lack of significant contribution from the PSF component suggests that a very compact stellar structure dominates GS-9209's emission only up to $\lambda_{\rm rest} \sim 2\mu m$, a conclusion independently reached by our SED analysis below. For F1500W and F1800W, flux contributions from the PSF and from the Sérsic component become comparable. The flux ratio of the PSF to the Sérsic component is 0.46 and 0.65 for F1500W and F1800W, respectively. This suggests the observed MIRI fluxes at $\lambda_{\rm rest} \sim 3 - 5\mu m$ are likely associated with two origins, i.e. AGN dust torus and the dust emission from diffuse ISM, a conclusion again independently reached by our SED analysis. We note, however, that with current F1500W and F1800W imaging, the reduced χ^2 between the single Sérsic fitting and the PSF+Sérsic fitting are statistically indistinguishable.

The PSF+Sérsic fitting returns $r_e = 2.4 \pm 0.6$ kpc in F1800W, with the best-fit Sérsic index of $n \sim 0.2$ which hits the minimal n commonly allowed in Sérsic modeling[63]. We therefore perform another PSF+Sérsic fitting by fixing $n = 1$ (exponential disk), which returns $r_e = 1.8 \pm 0.5$ kpc in F1800W, i.e. ≈ 10 times of the stellar r_e.

We note that, relative to the single Sérsic fitting, this significant increase in r_e derived from the PSF+Sérsic fitting is expected, because adding a PSF is equivalent to fitting the F1800W image of GS-9209 with some fraction of central (non-stellar) flux removed. We also note that, unlike the r_e from the single Sérsic fitting which is a characteristic size of total hot dust emission regardless of its origin, the r_e from the PSF+Sérsic fitting should be considered as the size of hot dust emission that is only associated with the diffuse ISM of GS-9209.

4 Analysis of spectral energy distribution

We perform detailed analysis of the spectral energy distribution (SED) of GS-9209 via SED modeling, with an emphasis on constraining the origin of the observed MIRI fluxes. Data included in the modeling is the photometry of 25 filters from HST/ACS (F435W, F606W, F775W, F814W and F850LP), JWST/NIRCam (F090W, F115W, F150W, F182M, F200W, F210M, F277W, F356W, F410M, F430M, F444W, F460M and F480M) and JWST/MIRI (F560W, F770W, F1000W, F1280W, F1500W, F1800W and F2100W). All photometry is measured using the PSF-matched images where all images are PSF-homogenized to MIRI/F2100W, the longest wavelength band where GS-9209 is detected. During our SED fitting, an error floor is imposed on photometry: the uncertainty of flux is not allowed to be smaller than 5%, the typical uncertainty caused by imperfect flux calibration and PSF homogenization.

The SED fitting is done mainly with the software PROSPECTOR[64]. The basic setups of our PROSPECTOR fitting are detailed as follows. We fix the redshift to be $z = 4.658$[10]. We use the Kroupa[65] stellar initial mass function. We adopt the FSPS stellar synthesis code[66,67] with the stellar isochrone libraries MIST[68,69] and the stellar spectral libraries MILES[70]. We use the Madau[71] IGM transmission model. We include the model of Byler et al.[72] for nebular emission. By default, we treat differently the dust attenuation towards nebular emission and young (< 10 Myr) stellar populations, and towards old (> 10 Myr) stellar populations[73]. The dust attenuation of the former is modelled as a power law, while the latter is modelled following the parameterization of Noll et al.[74], i.e., a modified Calzetti et al.[75] dust attenuation law with a Lorentzian-like profile to describe the 2175Å dust feature. Following Kriek and Conroy[76], we tie the strength of the 2175Å feature to the dust index of Noll et al.[74].

For the fiducial star formation history (SFH), we use a nonparametric, piece-wise form composed of 9 lookback time bins with the continuity prior[77]. The first three lookback time bins are fixed to be $0 - 10$, $10 - 30$ and $30 - 100$ Myr to capture recent episodes of star formation with relatively high time resolution. The last lookback time bin is $0.9t_H - t_H$ where t_H is the Hubble Time at $z = 4.658$. The remaining five bins are evenly spaced in logarithmic space between 100 Myr and $0.9t_H$. Such a choice of lookback time bins is very similar to those extensively used in recent studies of high-redshift massive galaxies[78,79,80,81,82]. Nonetheless, in a later Section, we still test our SED fitting results using different time bins of nonparametric SFH.

With photometric data alone, it remains difficult to tightly constrain stellar and gas-phase metallicities. By default, we thus use strong priors based on the metallicity measures and their uncertainties from NIRSpec spectroscopy of Carnall et al.[10].

Specifically, for stellar metallicity, we assume a Gaussian prior centered at $0.11Z_\odot$ with a width of 0.1 dex. For gas-phase metallicity, we assume a Gaussian prior centered at $0.17Z_\odot$ with a width of 1 dex. We shall test our SED fitting results using different metallicity assumptions in a later Section.

The MIRI imaging covers the spectral range of GS-9209 towards $\lambda_{\rm rest} \sim 3-5\mu m$ where hot dust emission, if present, becomes increasingly important[83,84]. We thus also add models of dust emission to the SED modeling (see below for details).

4.1 SED modeling of the entire galaxy

We start by fitting the SED of GS-9209 using integrated photometry, i.e. total flux within a circular aperture of $r = 0.7$" which is about the size of the galaxy's extent in the segmentation map. For dust emission, here we use models of Nenkova et al.[85],[86] to model the emission from AGN dust torus, and of Draine and Li[27] to model the reprocessed emission of dust associated with diffuse ISM. These two models are the default of PROSPECTOR and have been widely used in the literature.

We do not include the results from this fitting of integrated photometry to the main text, as this analysis is mainly served as a consistency check with the previous inference of GS-9209's stellar-population properties done by Carnall et al.[10] who performed the SED fitting mainly with the JWST/NIRSpec fixed-slit spectroscopy with medium resolution gratings of G235M and G395M.

The left panel of Fig. 7 shows the SED fitting result of integrated photometry. The best-fit model shows a strong rest-frame 4000Å break and prominent absorption features associated with A-type stars, in line with the NIRSpec spectroscopy of Carnall et al.[10] confirming the quiescent/post-starburst nature of GS-9209. More importantly, with MIRI photometry, it immediately becomes clear that the hot dust emission is required to reproduce the SED of GS-9209 at $\lambda_{\rm rest} > 2\mu m$. The origin of the hot dust emission will be elaborated in greater detail in following Sections through analysis of the inner and outer regions of GS-9209.

Using integrated photometry, we obtain a stellar mass of $\log_{10}(M_*/M_\odot) = 10.62^{+0.03}_{-0.02}$, in excellent agreement with that ($\log_{10}(M_*/M_\odot) = 10.58 \pm 0.02$) measured by Carnall et al.[10] using NIRSpec spectroscopy.

We obtain a star formation rate of SFR $= 2.7^{+3.0}_{-2.4}\,M_\odot/{\rm yr}$. The SFR from SED fitting can be sensitive to the assumed SFH[84]. If we use a parametric delayed-tau SFH, i.e. SFR(t) $\propto {\rm te}^{-{\rm t}/\tau}$, we would obtain SFR $= 1.0^{+2.6}_{-0.8}\,M_\odot/{\rm yr}$. We note that our SED-inferred SFR, no matter which SFH is assumed, is larger than that inferred from the SED fitting of Carnall et al.[10] which suggested that the SFR of GS-9209 is consistent with zero over the past 100 Myr. Interestingly, however, our SFR is actually in excellent agreement with what is inferred based on the narrow component of Hα emission (SFR$_{\rm H\alpha,narrow} = 1.9 \pm 0.1 M_\odot/{\rm yr}$) in the NIRSpec spectrum of Carnall et al.[10]. We mention that, even with the higher SFR from our measurement, the specific star formation rate (sSFR) of GS-9209 remains to be very low, i.e. $\log_{10}({\rm sSFR}/{\rm yr}^{-1}) = -10.1^{+0.5}_{-0.4}$ corresponding to $\sim 0.1/t_{\rm H}$ which is smaller than the sSFR threshold of $0.2/t_{\rm H}$ normally used for identifying quiescent galaxies at high redshift[87].

Finally, in the right panel of Fig. 7, we compare the reconstructed SFH of our measurement with that of Carnall et al.[10]. Overall, the two SFHs are similar: The
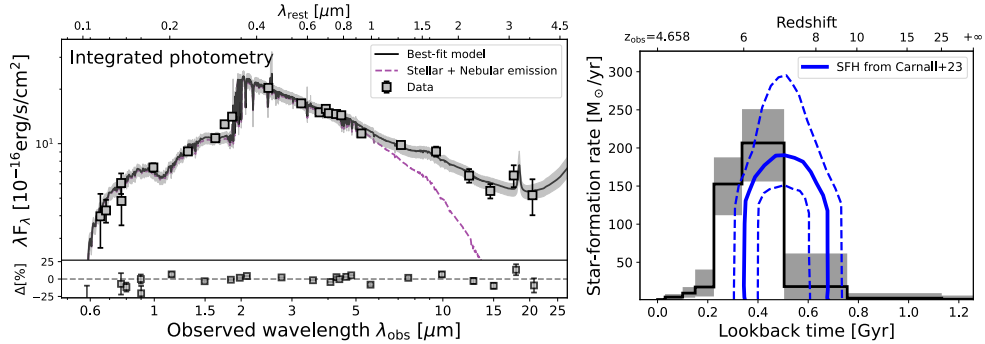
15

Fig. 7 SED fitting of the integrated photometry of GS-9209. The left panel shows the comparison between the best-fit model and data. The magenta dashed line shows the emission from the stellar and nebular emission of GS-9209. The dust emission is clearly required to reproduce the observed MIRI fluxes. The right panel shows the reconstructed SFH of GS-9209. For comparison, we plot in blue the SFH (both the best-fit and 1σ uncertainty) measured by Carnall et al.[10] using NIRSpec spectroscopy.

major stellar mass assembly of GS-9209 started ~ 500 Myr ago, i.e. $z \sim 7$, with a peak star formation rate $SFR_{peak} \sim 200 M_{\odot}/\mathrm{yr}$. Noticeably, however, the stellar population of GS-9209 inferred from our SED fitting is younger than that from Carnall et al.[10] by ~ 100 Myr (mass-weighted stellar age). We note that NIRSpec's fixed slit (S200A1) only has a width of 0".2, while in this work we find that GS-9209's outskirts are younger than its center. This can explain the younger stellar population found by our SED fitting of integrated photometry ($r = 0$".7 aperture).

4.2 SED modeling of the inner region

Here we describe our SED analysis of the inner region of GS-9209. The inner region is enclosed by an $r = 0$".3 (similar to the FWHM of MIRI/F2100W image) circular aperture centered at the centroid of F770W, i.e. the stellar continuum of GS-9209.

For dust emission, by default we use the same models as used for the SED fitting of integrated photometry (Section 4.1). The results have been presented in Fig. 4 and discussed in detail in the main text. In what follows, we alter our SED modeling significantly to check that if our conclusion about the origin of MIRI fluxes is sensitive to the default SED assumptions.

First, we replace both the default Draine and Li[27] dust model and the Nenkova et al.[85],[86] AGN torus model with the semi-empirical dust emission models of Lyu et al.[88]. The Lyu et al.[88] templates are calibrated against various observations both for UV-to-IR AGN emission and for galaxy dust emission associated diffuse ISM[89,88]. Second, because of the highly uncertain dust extinction of AGN, instead of assuming the same dust attenuation law for both, following Lyu et al.[88], we use two different dust laws, namely, the dust attenuation law of Calzetti et al.[75] for the host galaxy and the dust extinction curve of SMC[90] for the AGN. Finally, instead of assuming a nonparametric SFH, we use a parametric delayed-tau SFH.
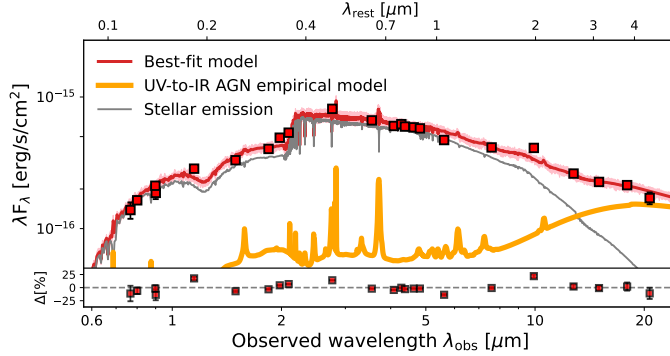
16

Fig. 8 Alternative SED fitting of the inner region of GS-9209. Despite that the SED model assumptions here differ greatly from the fiducial ones used in the main text (see Section 4.2 for details), our key conclusions stand: For the inner region of GS-9209, the observed MIRI fluxes (1) require the addition of hot dust emission to reproduce and (2) are dominated by the dust emission of AGN.

Fig. 8 shows the fitting results of the alternative SED modeling. To begin, unlike the Nenkova et al. [85],[86] model which only includes the contribution from AGN torus, the semi-empirical templates of Lyu et al. [88] actually also include the UV-to-optical AGN emission. Yet, the fitting still suggests that the rest-UV to NIR emission of GS-9209 is dominated by starlight. At $\lambda_{\rm rest} \gtrsim 2\mu m$, similar to what we found in the fiducial modeling, the observed MIRI fluxes cannot be reproduced by the alternative model with stellar emission alone, i.e. the need for dust emission. We remind that the dust emission of diffuse ISM is included to the alternative SED modeling. Nonetheless, the fitting still suggests that GS-9209's SED at $\lambda_{\rm rest} \gtrsim 3\mu m$ is dominated by the dust emission of AGN torus, in line with the fiducial modeling. It is also worth mentioning that based on our SED fitting we estimate the AGN luminosity of GS-9209 at rest-frame 5100Å to be $L_{5100} = 10^{10.17} L_\odot$ which is in great agreement with that independently estimated by Carnall et al. [10] who obtained $L_{5100} \sim 10^{10} L_\odot$ by SED fitting using the NIRSpec spectrum or $L_{5100} \sim 10^{10.2} L_\odot$ by converting the observed broad Hα flux using the relation of Greene and Ho [91].

Finally, another line of evidence that the inner MIRI fluxes of GS-9209 at $\lambda_{\rm rest} \gtrsim 3\mu m$ is dominated by AGN comes from additional SED fitting where we switch off the AGN component. Without the AGN component, the best-fit SED has the total (i.e. summation of all bands) $\chi^2_{tot} = 56.3$, which, as expected, is worse compared to $\chi^2_{tot} = 37.4$ of the best-fit model with AGN switched on. More importantly, with the assumption of energy balance, i.e. the energy absorbed by dust in the rest-frame UV is re-emitted in the IR, such a fitting forces to use the dust emission associated with diffuse ISM (i.e. star formation) to explain the observed MIRI fluxes. As a result, this fitting returns SFR $= 50 \pm 5 M_\odot/{\rm yr}$, which is significantly higher than both that inferred from the narrow Hα emission [10] (SFR$_{{\rm H}\alpha,{\rm narrow}} \sim 2 M_\odot/{\rm yr}$), and the strict upper limit set by archival ALMA non-detections of GS-9209 [92] (SFR$_{\rm ALMA} <$ $41 M_\odot/{\rm yr}$). These together strongly argue against the origin of the observed MIRI fluxes to be dominated by the dust emission associated with diffuse ISM.
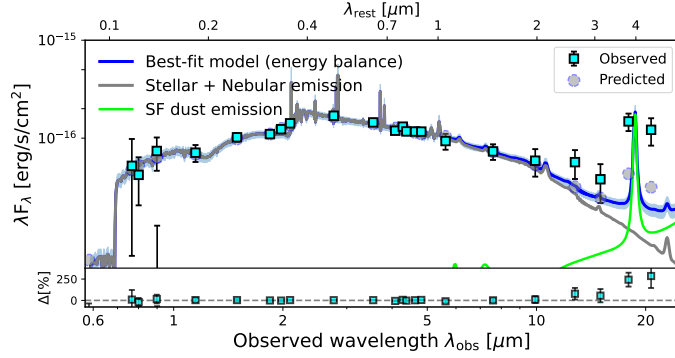
17

Fig. 9 SED fitting of the outer region of GS-9209 with the assumption of energy balance. The observed MIRI fluxes at $\lambda_{\mathrm{obs}} > 10\mu m$ are not well fitted under this assumption.

To summarize, the assumptions made in the above alternative SED modelings differ greatly from the fiducial ones, which we did intentionally. Yet, they reach to the conclusions fully in line with the fiducial SED fitting. Therefore, we conclude that our results regarding the origin of MIRI fluxes of GS-9209's inner region – AGN dominated – are not sensitive to the SED assumptions.

4.3 SED modeling of the outer region

Here we describe our SED analysis of the outer region of GS-9209. The outer region is enclosed by a 0"3 $< r <$ 0.7" circular annulus aperture. Due to PSF broadening, we subtract the flux contribution from the inner part to the outer aperture by assuming the inner component is a point source, which is a good approximation because the surface brightness profile of GS-9209's inner part is very similar to PSF (Fig. 2). As the flux contribution from the inner region to the outer aperture has been removed, the AGN component is not included to the SED fitting of the outer region.

To begin, we run SED fitting with the assumption of energy balance. By default, we use the Draine and Li[27] model. As Fig. 9 shows, the observed MIRI fluxes at $\lambda_{\mathrm{obs}} > 10\mu m$, or $\lambda_{\mathrm{rest}} > 2.5\mu m$, cannot be fitted well. This issue cannot be mitigated by replacing the Draine and Li[27] model with other (semi-)empirical dust models extensively used in the literature, e.g.[28,29]. Further, we test the finding by using a different stellar synthesis code BC03[93] and SED fitting software BAGPIPES[94]. These changes do not help to mitigate the issue, either. As detailed in the main text, however, this issue can be largely mitigated, if not fully resolved, by removing the energy balance assumption.

4.4 Tests on other SED assumptions

We now investigate the impact of other SED assumptions on the key conclusions of our SED analysis, namely that the outer region of GS-9209 is younger and more dust attenuated than its inner region. The results are plotted in Fig. 10. Specifically, we test the assumptions of:
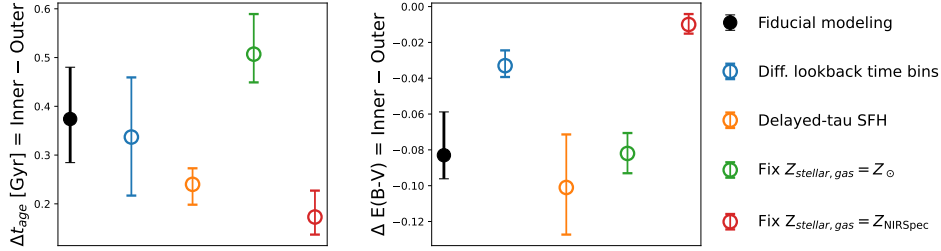
Fig. 10 The differences in stellar age and $E(B-V)$ between GS-9209's inner and outer regions from SED fittings with SFH and metallicity assumptions differing from the fiducial ones. Our conclusions do not change: The outer region of GS-9209 is younger ($\Delta t_{\mathrm{age}} > 0$) and more dust attenuated ($\Delta E(B-V) < 0$) than its inner region.

- SFH. We test our results by using two other different forms of SFH, namely (1) a parametric delayed-tau SFH and (2) a nonparametric continuity SFH with lookback time bins different from the fiducial ones (here the nine lookback time bins are assumed to be $0-30$ and $30-100$ Myr for the first two bins; $0.85t_{\mathrm{H}} - t_{\mathrm{H}}$ for the last bin; and evenly spaced in the logarithmic lookback time between 100 Myr and $0.85t_{\mathrm{H}}$ for the remaining six bins). As Fig. 10 (blue and orange circles) shows, we do not see any substantial changes in our conclusions by altering the assumed SFH.
- metallicities. Instead of setting the stellar and gas-phase metallicities of GS-9209 to be free parameters, we assume that the inner and outer regions have the same metallicities and we fix them to be either (1) the best-fit values measured with NIRSpec spectroscopy[10] or (2) the solar values. We note that, according to its NIRSpec spectrum, the stellar metallicity of GS-9209 should be substantially lower than the solar value[10] and there is no evidence that the metallicities of the inner and outer regions are the same. As Fig. 10 (green and red circles) shows, even with these arguably "bad" metallicity assumptions, we still find that the outer region of GS-9209 is younger and more dust attenuated than its inner region, showing that our conclusions are not sensitive to the assumed metallicities.

Acknowledgments

Author contributions

ZJ, CCW, GHR, JL and SA contributed to the initial discovery. All authors contributed to the interpretation of results. ZJ, JL and JMH contributed to the analysis of Spectral Energy Distribution. ZJ, CCW and FS contributed to the morphological analysis. GHR, JL, SA, IS, YZ contributed to the design and data reduction of the MIRI imaging of the SMILES program. MR, FS, FD, ST, BR, RM, AJB and CNAW contributed to the design and data reduction of the NIRCam imaging of the JADES program. CCW and ST contributed to the design and data reduction of the NIRCam imaging of the JEMS program.

References

[1] Ji, Z., Williams, C.C., Suess, K.A., Tacchella, S., Johnson, B.D., Robertson, B., Alberts, S., Baker, W.M., Baum, S., Bhatawdekar, R., Bonaventura, N., Boyett, K., Bunker, A.J., Carniani, S., Charlot, S., Chen, Z., Chevallard, J., Curtis-Lake, E., D'Eugenio, F., de Graaff, A., DeCoursey, C., Egami, E., Eisenstein, D.J., Hainline, K., Hausen, R., Helton, J.M., Looser, T.J., Lyu, J., Maiolino, R., Maseda, M.V., Nelson, E., Rieke, G., Rieke, M., Rix, H.-W., Sandles, L., Sun, F., Übler, H., Willmer, C.N.A., Willott, C., Witstok, J.: JADES: Rest-frame UV-to-NIR Size Evolution of Massive Quiescent Galaxies from Redshift z=5 to z=0.5. arXiv e-prints, 2401–00934 (2024) https://doi.org/10.48550/arXiv.2401.00934 arXiv:2401.00934 [astro-ph.GA]

[2] Merlin, E., Chiosi, C., Piovan, L., Grassi, T., Buonomo, U., La Barbera, F.: Formation and evolution of early-type galaxies - III. Dependence of the star formation history on the total mass and initial overdensity. Mon. Not. R. Astron. Soc. **427**(2), 1530–1554 (2012) https://doi.org/10.1111/j.1365-2966.2012.21965.x arXiv:1204.5118 [astro-ph.CO]

[3] Chiosi, C., Merlin, E., Piovan, L., Tantalo, R.: Monolithic View of Galaxy Formation and Evolution. Galaxies **2**(3), 300–381 (2014) https://doi.org/10.3390/galaxies2030300

[4] Glazebrook, K., Nanayakkara, T., Schreiber, C., Lagos, C., Kawinwanichakij, L., Jacobs, C., Chittenden, H., Brammer, G., Kacprzak, G.G., Labbe, I., Marchesini, D., Marsan, Z.C., Oesch, P.A., Papovich, C., Remus, R.-S., Tran, K.-V.H., Esdaile, J., Chandro Gomez, A.: A massive galaxy that formed its stars at $z \sim$

11. arXiv e-prints, 2308–05606 (2023) https://doi.org/10.48550/arXiv.2308.05606 arXiv:2308.05606 [astro-ph.GA]

[5] de Graaff, A., Setton, D.J., Brammer, G., Cutler, S., Suess, K.A., Labbe, I., Leja, J., Weibel, A., Maseda, M.V., Whitaker, K.E., Bezanson, R., Boogaard, L.A., Cleri, N.J., De Lucia, G., Franx, M., Greene, J.E., Hirschmann, M., Matthee, J., McConachie, I., Naidu, R.P., Oesch, P.A., Price, S.H., Rix, H.-W., Valentino, F., Wang, B., Williams, C.C.: Efficient formation of a massive quiescent galaxy at redshift 4.9. arXiv e-prints, 2404–05683 (2024) https://doi.org/10.48550/arXiv.2404.05683 arXiv:2404.05683 [astro-ph.GA]

[6] Nanayakkara, T., Glazebrook, K., Jacobs, C., Kawinwanichakij, L., Schreiber, C., Brammer, G., Esdaile, J., Kacprzak, G.G., Labbe, I., Lagos, C., Marchesini, D., Marsan, Z.C., Oesch, P.A., Papovich, C., Remus, R.-S., Tran, K.-V.H.: A population of faint, old, and massive quiescent galaxies at 3 ¡z ¡4 revealed by JWST NIRSpec Spectroscopy. Scientific Reports **14**, 3724 (2024) https://doi.org/10.1038/s41598-024-52585-4 arXiv:2212.11638 [astro-ph.GA]

[7] Weibel, A., de Graaff, A., Setton, D.J., Miller, T.B., Oesch, P.A., Brammer, G., Lagos, C.D.P., Whitaker, K.E., Williams, C.C., Baggen, J.F.W., Bezanson, R., Boogaard, L.A., Cleri, N.J., Greene, J.E., Hirschmann, M., Hviding, R.E., Kuruvanthodi, A., Labbé, I., Leja, J., Maseda, M.V., Matthee, J., McConachie, I., Naidu, R.P., Roberts-Borsani, G., Schaerer, D., Suess, K.A., Valentino, F., van Dokkum, P., Wang, B.: RUBIES Reveals a Massive Quiescent Galaxy at z=7.3. arXiv e-prints, 2409–03829 (2024) https://doi.org/10.48550/arXiv.2409.03829 arXiv:2409.03829 [astro-ph.GA]

[8] Gould, K.M.L., Brammer, G., Valentino, F., Whitaker, K.E., Weaver, J.R., Lagos, C.d.P., Rizzo, F., Franco, M., Hsieh, B.-C., Ilbert, O., Jin, S., Magdis, G., McCracken, H.J., Mobasher, B., Shuntov, M., Steinhardt, C.L., Strait, V., Toft, S.: COSMOS2020: Exploring the Dawn of Quenching for Massive Galaxies at 3 ¡ z ¡ 5 with a New Color-selection Method. Astron. J. **165**(6), 248 (2023) https://doi.org/10.3847/1538-3881/accadc arXiv:2302.10934 [astro-ph.GA]

[9] Valentino, F., Brammer, G., Gould, K.M.L., Kokorev, V., Fujimoto, S., Jespersen, C.K., Vijayan, A.P., Weaver, J.R., Ito, K., Tanaka, M., Ilbert, O., Magdis, G.E., Whitaker, K.E., Faisst, A.L., Gallazzi, A., Gillman, S., Giménez-Arteaga, C., Gómez-Guijarro, C., Kubo, M., Heintz, K.E., Hirschmann, M., Oesch, P., Onodera, M., Rizzo, F., Lee, M., Strait, V., Toft, S.: An Atlas of Color-selected Quiescent Galaxies at z ¿ 3 in Public JWST Fields. Astrophys. J. **947**(1), 20 (2023) https://doi.org/10.3847/1538-4357/acbefa arXiv:2302.10936 [astro-ph.GA]

[10] Carnall, A.C., McLure, R.J., Dunlop, J.S., McLeod, D.J., Wild, V., Cullen, F., Magee, D., Begley, R., Cimatti, A., Donnan, C.T., Hamadouche, M.L., Jewell, S.M., Walker, S.: A massive quiescent galaxy at redshift 4.658. Nature **619**(7971),

716–719 (2023) https://doi.org/10.1038/s41586-023-06158-6 arXiv:2301.11413 [astro-ph.GA]

[11] Grudić, M.Y., Hopkins, P.F., Quataert, E., Murray, N.: The maximum stellar surface density due to the failure of stellar feedback. Mon. Not. R. Astron. Soc. **483**(4), 5548–5553 (2019) https://doi.org/10.1093/mnras/sty3386 arXiv:1804.04137 [astro-ph.GA]

[12] Wright, G.S., Rieke, G.H., Glasse, A., Ressler, M., García Marín, M., Aguilar, J., Alberts, S., Álvarez-Márquez, J., Argyriou, I., Banks, K., Baudoz, P., Boccaletti, A., Bouchet, P., Bouwman, J., Brandl, B.R., Breda, D., Bright, S., Cale, S., Colina, L., Cossou, C., Coulais, A., Cracraft, M., De Meester, W., Dicken, D., Engesser, M., Etxaluze, M., Fox, O.D., Friedman, S., Fu, H., Gasman, D., Gáspár, A., Gastaud, R., Geers, V., Glauser, A.M., Gordon, K.D., Greene, T., Greve, T.R., Grundy, T., Güdel, M., Guillard, P., Haderlein, P., Hashimoto, R., Henning, T., Hines, D., Holler, B., Detre, Ö.H., Jahromi, A., James, B., Jones, O.C., Justtanont, K., Kavanagh, P., Kendrew, S., Klaassen, P., Krause, O., Labiano, A., Lagage, P.-O., Lambros, S., Larson, K., Law, D., Lee, D., Libralato, M., Lorenzo Alverez, J., Meixner, M., Morrison, J., Mueller, M., Murray, K., Mycroft, M., Myers, R., Nayak, O., Naylor, B., Nickson, B., Noriega-Crespo, A., Östlin, G., O'Sullivan, B., Ottens, R., Patapis, P., Penanen, K., Pietraszkiewicz, M., Ray, T., Regan, M., Roteliuk, A., Royer, P., Samara-Ratna, P., Samuelson, B., Sargent, B.A., Scheithauer, S., Schneider, A., Schreiber, J., Shaughnessy, B., Sheehan, E., Shivaei, I., Sloan, G.C., Tamas, L., Teague, K., Temim, T., Tikkanen, T., Tustain, S., van Dishoeck, E.F., Vandenbussche, B., Weilert, M., Whitehouse, P., Wolff, S.: The Mid-infrared Instrument for JWST and Its In-flight Performance. PASP **135**(1046), 048003 (2023) https://doi.org/10.1088/1538-3873/acbe66

[13] Gardner, J.P., Mather, J.C., Abbott, R., Abell, J.S., Abernathy, M., Abney, F.E., Abraham, J.G., Abraham, R., Abul-Huda, Y.M., Acton, S., Adams, C.K., Adams, E., Adler, D.S., Adriaensen, M., Aguilar, J.A., Ahmed, M., Ahmed, N.S., Ahmed, T., Albat, R., Albert, L., Alberts, S., Aldridge, D., Allen, M.M., Allen, S.S., Altenburg, M., Altunc, S., Alvarez, J.L., Álvarez-Márquez, J., Alves de Oliveira, C., Ambrose, L.L., Anandakrishnan, S.M., Andersen, G.C., Anderson, H.J., Anderson, J., Anderson, K., Anderson, S.M., Aprea, J., Archer, B.J., Arenberg, J.W., Argyriou, I., Arribas, S., Artigau, É., Arvai, A.R., Atcheson, P., Atkinson, C.B., Averbukh, J., Aymergen, C., Bacinski, J.J., Baggett, W.E., Bagnasco, G., Baker, L.L., Balzano, V.A., Banks, K.A., Baran, D.A., Barker, E.A., Barrett, L.K., Barringer, B.O., Barto, A., Bast, W., Baudoz, P., Baum, S., Beatty, T.G., Beaulieu, M., Bechtold, K., Beck, T., Beddard, M.M., Beichman, C., Bellagama, L., Bely, P., Berger, T.W., Bergeron, L.E., Bernier, A.-D., Bertch, M.D., Beskow, C., Betz, L.E., Biagetti, C.P., Birkmann, S., Bjorklund, K.F., Blackwood, J.D., Blazek, R.P., Blossfeld, S., Bluth, M., Boccaletti, A., Boegner, J. Martin E., Bohlin, R.C., Boia, J.J., Böker, T., Bonaventura, N., Bond, N.A., Bosley, K.A., Boucarut, R.A., Bouchet, P., Bouwman, J., Bower, G., Bowers, A.S., Bowers, C.W., Boyce, L.A., Boyer, C.T., Boyer, M.L., Boyer, M., Boyer, R., Bradley, L.D.,

Brady, G.R., Brandl, B.R., Brannen, J.L., Breda, D., Bremmer, H.G., Brennan, D., Bresnahan, P.A., Bright, S.N., Broiles, B.J., Bromenschenkel, A., Brooks, B.H., Brooks, K.J., Brown, B., Brown, B., Brown, T.M., Bruce, B.W., Bryson, J.G., Bujanda, E.D., Bullock, B.M., Bunker, A.J., Bureo, R., Burt, I.J., Bush, J.A., Bushouse, H.A., Bussman, M.C., Cabaud, O., Cale, S., Calhoon, C.D., Calvani, H., Canipe, A.M., Caputo, F.M., Cara, M., Carey, L., Case, M.E., Cesari, T., Cetorelli, L.D., Chance, D.R., Chandler, L., Chaney, D., Chapman, G.N., Charlot, S., Chayer, P., Cheezum, J.I., Chen, B., Chen, C.H., Cherinka, B., Chichester, S.C., Chilton, Z.S., Chittiraibalan, D., Clampin, M., Clark, C.R., Clark, K.W., Clark, S.M., Claybrooks, E.E., Cleveland, K.A., Cohen, A.L., Cohen, L.M., Colón, K.D., Coleman, B.L., Colina, L., Comber, B.J., Comeau, T.M., Comer, T., Conde Reis, A., Connolly, D.C., Conroy, K.E., Contos, A.R., Contreras, J., Cook, N.J., Cooper, J.L., Cooper, R.A., Correia, M.F., Correnti, M., Cossou, C., Costanza, B.F., Coulais, A., Cox, C.R., Coyle, R.T., Cracraft, M.M., Crew, K.A., Curtis, G.J., Cusveller, B., Da Costa Maciel, C., Dailey, C.T., Daugeron, F., Davidson, G.S., Davies, J.E., Davis, K.A., Davis, M.S., Day, R., de Chambure, D., de Jong, P., De Marchi, G., Dean, B.H., Decker, J.E., Delisa, A.S., Dell, L.C., Dellagatta, G., Dembinska, F., Demosthenes, S., Dencheva, N.M., Deneu, P., DePriest, W.W., Deschenes, J., Dethienne, N., Detre, Ö.H., Diaz, R.I., Dicken, D., DiFelice, A.S., Dillman, M., Disharoon, M.O., Dixon, W.V., Doggett, J.B., Dominguez, K.L., Donaldson, T.S., Doria-Warner, C.M., Santos, T.D., Doty, H., Douglas, J. Robert E., Doyon, R., Dressler, A., Driggers, J., Driggers, P.A., Dunn, J.L., DuPrie, K.C., Dupuis, J., Durning, J., Dutta, S.B., Earl, N.M., Eccleston, P., Ecobichon, P., Egami, E., Ehrenwinkler, R., Eisenhamer, J.D., Eisenhower, M., Eisenstein, D.J., El Hamel, Z., Elie, M.L., Elliott, J., Elliott, K.W., Engesser, M., Espinoza, N., Etienne, O., Etxaluze, M., Evans, L., Fabreguettes, L., Falcolini, M., Falini, P.R., Fatig, C., Feeney, M., Feinberg, L.D., Fels, R., Ferdous, N., Ferguson, H.C., Ferrarese, L., Ferreira, M.-H., Ferruit, P., Ferry, M., Filippazzo, J.C., Firre, D., Fix, M., Flagey, N., Flanagan, K.A., Fleming, S.W., Florian, M., Flynn, J.R., Foiadelli, L., Fontaine, M.R., Fontanella, E.M., Forshay, P.R., Fortner, E.A., Fox, O.D., Framarini, A.P., Francisco, J.I., Franck, R., Franx, M., Franz, D.E., Friedman, S.D., Friend, K.E., Frost, J.R., Fu, H., Fullerton, A.W., Gaillard, L., Galkin, S., Gallagher, B., Galyer, A.D., García Marín, M., Gardner, L.E., Garland, D., Garrett, B.A., Gasman, D., Gáspár, A., Gastaud, R., Gaudreau, D., Gauthier, P.T., Geers, V., Geithner, P.H., Gennaro, M., Gerber, J., Gereau, J.C., Giampaoli, R., Giardino, G., Gibbons, P.C., Gilbert, K., Gilman, L., Girard, J.H., Giuliano, M.E., Gkountis, K., Glasse, A., Glassmire, K.Z., Glauser, A.M., Glazer, S.D., Goldberg, J., Golimowski, D.A., Gonzaga, S.P., Gordon, K.D., Gordon, S.J., Goudfrooij, P., Gough, M.J., Graham, A.J., Grau, C.M., Green, J.D., Greene, G.R., Greene, T.P., Greenfield, P.E., Greenhouse, M.A., Greve, T.R., Greville, E.M., Grimaldi, S., Groe, F.E., Groebner, A., Grumm, D.M., Grundy, T., Güdel, M., Guillard, P., Guldalian, J., Gunn, C.A., Gurule, A., Gutman, I.M., Guy, P.D., Guyot, B., Hack, W.J., Haderlein, P., Hagan, J.B., Hagedorn, A., Hainline, K., Haley, C., Hami, M., Hamilton, F.C., Hammann, J., Hammel, H.B., Hanley, C.J., Hansen, C.A., Hardy, B., Harnisch, B., Harr, M.H., Harris,

P., Hart, J.A., Hartig, G.F., Hasan, H., Hashim, K.M., Hashimoto, R., Haskins, S.J., Hawkins, R.E., Hayden, B., Hayden, W.L., Healy, M., Hecht, K., Heeg, V.J., Hejal, R., Helm, K.A., Hengemihle, N.J., Henning, T., Henry, A., Henry, R.L., Henshaw, K., Hernandez, S., Herrington, D.C., Heske, A., Hesman, B.E., Hickey, D.L., Hilbert, B.N., Hines, D.C., Hinz, M.R., Hirsch, M., Hitcho, R.S., Hodapp, K., Hodge, P.E., Hoffman, M., Holfeltz, S.T., Holler, B.J., Hoppa, J.R., Horner, S., Howard, J.M., Howard, R.J., Huber, J.M., Hunkeler, J.S., Hunter, A., Hunter, D.G., Hurd, S.W., Hurst, B.J., Hutchings, J.B., Hylan, J.E., Ignat, L.I., Illingworth, G., Irish, S.M., Isaacs, I. John C., Jackson, J. Wallace C., Jaffe, D.T., Jahic, J., Jahromi, A., Jakobsen, P., James, B., James, J.C., James, L.R., Jamieson, W.B., Jandra, R.D., Jayawardhana, R., Jedrzejewski, R., Jeffers, B.S., Jensen, P., Joanne, E., Johns, A.T., Johnson, C.A., Johnson, E.L., Johnson, P., Johnson, P.S., Johnson, T.K., Johnson, T.W., Johnstone, D., Jollet, D., Jones, D.P., Jones, G.S., Jones, O.C., Jones, R.A., Jones, V., Jordan, I.J., Jordan, M.E., Jue, R., Jurkowski, M.H., Justis, G., Justtanont, K., Kaleida, C.C., Kalirai, J.S., Kalmanson, P.C., Kaltenegger, L., Kammerer, J., Kan, S.K., Kanarek, G.C., Kao, S.-H., Karakla, D.M., Karl, H., Kassin, S.A., Kauffman, D.D., Kavanagh, P., Kelley, L.L., Kelly, D.M., Kendrew, S., Kennedy, H.V., Kenny, D.A., Keski-Kuha, R.A., Keyes, C.D., Khan, A., Kidwell, R.C., Kimble, R.A., King, J.S., King, R.C., Kinzel, W.M., Kirk, J.R., Kirkpatrick, M.E., Klaassen, P., Klingemann, L., Klintworth, P.U., Knapp, B.A., Knight, S., Knollenberg, P.J., Knutsen, D.M., Koehler, R., Koekemoer, A.M., Kofler, E.T., Kontson, V.L., Kovacs, A.R., Kozhurina-Platais, V., Krause, O., Kriss, G.A., Krist, J., Kristoffersen, M.R., Krogel, C., Krueger, A.P., Kulp, B.A., Kumari, N., Kwan, S.W., Kyprianou, M., Labador, A.G., Labiano, Á., Lafrenière, D., Lagage, P.-O., Laidler, V.G., Laine, B., Laird, S., Lajoie, C.-P., Lallo, M.D., Lam, M.Y., LaMassa, S.M., Lambros, S.D., Lampenfield, R.J., Lander, M.E., Langston, J.H., Larson, K., Larson, M., LaVerghetta, R.J., Law, D.R., Lawrence, J.F., Lee, D.W., Lee, J., Lee, Y.-N.P., Leisenring, J., Leveille, M.D., Levenson, N.A., Levi, J.S., Levine, M.B., Lewis, D., Lewis, J., Lewis, N., Libralato, M., Lidon, N., Liebrecht, P.L., Lightsey, P., Lilly, S., Lim, F.C., Lim, P.L., Ling, S.-K., Link, L.J., Link, M.N., Lipinski, J.L., Liu, X., Lo, A.S., Lobmeyer, L., Logue, R.M., Long, C.A., Long, D.R., Long, I.D., Long, K.S., López-Caniego, M., Lotz, J.M., Love-Pruitt, J.M., Lubskiy, M., Luers, E.B., Luetgens, R.A., Luevano, A.J., Lui, S.M.G.F., Lund, I. James M., Lundquist, R.A., Lunine, J., Lützgendorf, N., Lynch, R.J., MacDonald, A.J., MacDonald, K., Macias, M.J., Macklis, K.I., Maghami, P., Maharaja, R.Y., Maiolino, R., Makrygiannis, K.G., Malla, S.G., Malumuth, E.M., Manjavacas, E., Marini, A., Marrione, A., Marston, A., Martel, A.R., Martin, D., Martin, P.G., Martinez, K.L., Maschmann, M., Masci, G.L., Masetti, M.E., Maszkiewicz, M., Matthews, G., Matuskey, J.E., McBrayer, G.A., McCarthy, D.W., McCaughrean, M.J., McClare, L.A., McClare, M.D., McCloskey, J.C., McClurg, T.D., McCoy, M., McElwain, M.W., McGregor, R.D., McGuffey, D.B., McKay, A.G., McKenzie, W.K., McLean, B., McMaster, M., McNeil, W., De Meester, W., Mehalick, K.L., Meixner, M., Meléndez, M., Menzel, M.P., Menzel, M.T., Merz, M., Mesterharm, D.D., Meyer, M.R., Meyett, M.L., Meza, L.E., Midwinter, C., Milam, S.N.,

24

Miller, J.T., Miller, W.C., Miskey, C.L., Misselt, K., Mitchell, E.P., Mohan, M., Montoya, E.E., Moran, M.J., Morishita, T., Moro-Martín, A., Morrison, D.L., Morrison, J., Morse, E.C., Moschos, M., Moseley, S.H., Mosier, G.E., Mosner, P., Mountain, M., Muckenthaler, J.S., Mueller, D.G., Mueller, M., Muhiem, D., Mühlmann, P., Mullally, S.E., Mullen, S.M., Munger, A.J., Murphy, J., Murray, K.T., Muzerolle, J.C., Mycroft, M., Myers, A., Myers, C.R., Myers, F.R.R., Myers, R., Myrick, K., Nagle, I. Adrian F., Nayak, O., Naylor, B., Neff, S.G., Nelan, E.P., Nella, J., Nguyen, D.T., Nguyen, M.N., Nickson, B., Nidhiry, J.J., Niedner, M.B., Nieto-Santisteban, M., Nikolov, N.K., Nishisaka, M.A., Noriega-Crespo, A., Nota, A., O'Mara, R.C., Oboryshko, M., O'Brien, M.B., Ochs, W.R., Offenberg, J.D., Ogle, P.M., Ohl, R.G., Olmsted, J.H., Osborne, S.B., O'Shaughnessy, B.P., Östlin, G., O'Sullivan, B., Otor, O.J., Ottens, R., Ouellette, N.N.-Q., Outlaw, D.J., Owens, B.A., Pacifici, C., Page, J.C., Paranilam, J.G., Park, S., Parrish, K.A., Paschal, L., Patapis, P., Patel, J., Patrick, K., Pattishall, J. Robert A., Paul, D.W., Paul, S.J., Pauly, T.A., Pavlovsky, C.M., Peña-Guerrero, M., Pedder, A.H., Peek, M.W., Pelham, P.A., Penanen, K., Perriello, B.A., Perrin, M.D., Perrine, R.F., Perrygo, C., Peslier, M., Petach, M., Peterson, K.A., Pfarr, T., Pierson, J.M., Pietraszkiewicz, M., Pilchen, G., Pipher, J.L., Pirzkal, N., Pitman, J.T., Player, D.M., Plesha, R., Plitzke, A., Pohner, J.A., Poletis, K.K., Pollizzi, J.A., Polster, E., Pontius, J.T., Pontoppidan, K., Porges, S.C., Potter, G.D., Prescott, S., Proffitt, C.R., Pueyo, L., Quispe Neira, I.A., Radich, A., Rager, R.T., Rameau, J., Ramey, D.D., Ramos Alarcon, R., Rampini, R., Rapp, R., Rashford, R.A., Rauscher, B.J., Ravindranath, S., Rawle, T., Rawlings, T.N., Ray, T., Regan, M.W., Rehm, B., Rehm, K.D., Reid, N., Reis, C.A., Renk, F., Reoch, T.B., Ressler, M., Rest, A.W., Reynolds, P.J., Richon, J.G., Richon, K.V., Ridgaway, M., Riedel, A.R., Rieke, G.H., Rieke, M.J., Rifelli, R.E., Rigby, J.R., Riggs, C.S., Ringel, N.J., Ritchie, C.E., Rix, H.-W., Robberto, M., Robinson, G.L., Robinson, M.S., Robinson, O., Rock, F.W., Rodriguez, D.R., Rodríguez del Pino, B., Roellig, T., Rohrbach, S.O., Roman, A.J., Romelfanger, F.J., Romo, J. Felipe P., Rosales, J.J., Rose, P., Roteliuk, A.F., Roth, M.N., Rothwell, B.Q., Rouzaud, S., Rowe, J., Rowlands, N., Roy, A., Royer, P., Rui, C., Rumler, P., Rumpl, W., Russ, M.L., Ryan, M.B., Ryan, R.M., Saad, K., Sabata, M., Sabatino, R., Sabbi, E., Sabelhaus, P.A., Sabia, S., Sahu, K.C., Saif, B.N., Salvignol, J.-C., Samara-Ratna, P., Samuelson, B.S., Sanders, F.A., Sappington, B., Sargent, B.A., Sauer, A., Savadkin, B.J., Sawicki, M., Schappell, T.M., Scheffer, C., Scheithauer, S., Scherer, R., Schiff, C., Schlawin, E., Schmeitzky, O., Schmitz, T.S., Schmude, D.J., Schneider, A., Schreiber, J., Schroeven-Deceuninck, H., Schultz, J.J., Schwab, R., Schwartz, C.H., Scoccimarro, D., Scott, J.F., Scott, M.B., Seaton, B.L., Seely, B.S., Seery, B., Seidleck, M., Sembach, K., Shanahan, C.E., Shaughnessy, B., Shaw, R.A., Shay, C.M., Sheehan, E., Sheth, K., Shih, H.-Y., Shivaei, I., Siegel, N., Sienkiewicz, M.G., Simmons, D.D., Simon, B.P., Sirianni, M., Sivaramakrishnan, A., Slade, J.E., Sloan, G.C., Slocum, C.E., Slowinski, S.E., Smith, C.T., Smith, E.P., Smith, E.C., Smith, K., Smith, R., Smith, S.J., Smolik, J.L., Soderblom, D.R., Sohn, S.T., Sokol, J., Sonneborn, G., Sontag, C.D., Sooy, P.R., Soummer, R., Southwood, D.M., Spain, K., Sparmo, J.,

Speer, D.T., Spencer, R., Sprofera, J.D., Stallcup, S.S., Stanley, M.K., Stansberry, J.A., Stark, C.C., Starr, C.W., Stassi, D.Y., Steck, J.A., Steeley, C.D., Stephens, M.A., Stephenson, R.J., Stewart, A.C., Stiavelli, M., , H.J. Stockman, Strada, P., Straughn, A.N., Streetman, S., Strickland, D.K., Strobele, J.F., Stuhlinger, M., Stys, J.E., Such, M., Sukhatme, K., Sullivan, J.F., Sullivan, P.C., Sumner, S.M., Sun, F., Sunnquist, B.D., Swade, D.A., Swam, M.S., Swenton, D.F., Swoish, R.A., Tam Litten, O.I., Tamas, L., Tao, A., Taylor, D.K., Taylor, J.M., te Plate, M., Van Tea, M., Teague, K.K., Telfer, R.C., Temim, T., Texter, S.C., Thatte, D.G., Thompson, C.L., Thompson, L.M., Thomson, S.R., Thronson, H., Tierney, C.M., Tikkanen, T., Tinnin, L., Tippet, W.T., Todd, C.W., Tran, H.D., Trauger, J., Trejo, E.G., Vinh Truong, J.H., Tsukamoto, C.L., Tufail, Y., Tumlinson, J., Tustain, S., Tyra, H., Ubeda, L., Underwood, K., Uzzo, M.A., Vaclavik, S., Valenduc, F., Valenti, J.A., Van Campen, J., van de Wetering, I., Van Der Marel, R.P., van Haarlem, R., Vandenbussche, B., van Dishoeck, E.F., Vanterpool, D.D., Vernoy, M.R., Vila Costas, M.B., Volk, K., Voorzaat, P., Voyton, M.F., Vydra, E., Waddy, D.J., Waelkens, C., Wahlgren, G.M., Walker, J. Frederick E., Wander, M., Warfield, C.K., Warner, G., Wasiak, F.C., Wasiak, M.F., Wehner, J., Weiler, K.R., Weilert, M., Weiss, S.B., Wells, M., Welty, A.D., Wheate, L., Wheeler, T.P., White, C.L., Whitehouse, P., Whiteleather, J.M., Whitman, W.R., Williams, C.C., Willmer, C.N.A., Willott, C.J., Willoughby, S.P., Wilson, A., Wilson, D., Wilson, D.V., Windhorst, R., Wislowski, E.C., Wolfe, D.J., Wolfe, M.A., Wolff, S., Wondel, A., Woo, C., Woods, R.T., Worden, E., Workman, W., Wright, G.S., Wu, C., Wu, C.-R., Wun, D.D., Wymer, K.B., Yadetie, T., Yan, I.C., Yang, K.C., Yates, K.L., Yeager, C.R., Yerger, E.J., Young, E.T., Young, G., Yu, G., Yu, S., Zak, D.S., Zeidler, P., Zepp, R., Zhou, J., Zincke, C.A., Zonak, S., Zondag, E.: The James Webb Space Telescope Mission. PASP **135**(1048), 068001 (2023) https://doi.org/10.1088/1538-3873/acd1b5 arXiv:2304.04869 [astro-ph.IM]

[14] Rieke, G., Alberts, S., Shivaei, I., Lyu, J., Willmer, C.N.A., Perez-Gonzalez, P., Williams, C.C.: The SMILES Mid-Infrared Survey. arXiv e-prints, 2406–03518 (2024) https://doi.org/10.48550/arXiv.2406.03518 arXiv:2406.03518 [astro-ph.GA]

[15] Alberts, S., Lyu, J., Shivaei, I., Rieke, G.H., Perez-Gonzalez, P.G., Bonventura, N., Zhu, Y., Helton, J.M., Ji, Z., Morrison, J., Robertson, B.E., Stone, M.A., Sun, Y., Williams, C.C., Willmer, C.N.A.: SMILES Initial Data Release: Unveiling the Obscured Universe with MIRI Multi-band Imaging. arXiv e-prints, 2405–15972 (2024) https://doi.org/10.48550/arXiv.2405.15972 arXiv:2405.15972 [astro-ph.GA]

[16] Sérsic, J.L.: Influence of the atmospheric and instrumental dispersion on the brightness distribution in a galaxy. Boletin de la Asociacion Argentina de Astronomia La Plata Argentina **6**, 41–43 (1963)

[17] Daddi, E., Renzini, A., Pirzkal, N., Cimatti, A., Malhotra, S., Stiavelli, M.,

Xu, C., Pasquali, A., Rhoads, J.E., Brusa, M., di Serego Alighieri, S., Ferguson, H.C., Koekemoer, A.M., Moustakas, L.A., Panagia, N., Windhorst, R.A.: Passively Evolving Early-Type Galaxies at 1.4 ¡~z ¡~2.5 in the Hubble Ultra Deep Field. Astrophys. J. **626**(2), 680–697 (2005) https://doi.org/10.1086/430104 arXiv:astro-ph/0503102 [astro-ph]

[18] Damjanov, I., McCarthy, P.J., Abraham, R.G., Glazebrook, K., Yan, H., Mentuch, E., Le Borgne, D., Savaglio, S., Crampton, D., Murowinski, R., Juneau, S., Carlberg, R.G., Jørgensen, I., Roth, K., Chen, H.-W., Marzke, R.O.: Red Nuggets at z ~1.5: Compact Passive Galaxies and the Formation of the Kormendy Relation. Astrophys. J. **695**(1), 101–115 (2009) https://doi.org/10.1088/0004-637X/695/1/101 arXiv:0807.1744 [astro-ph]

[19] Cassata, P., Giavalisco, M., Guo, Y., Renzini, A., Ferguson, H., Koekemoer, A.M., Salimbeni, S., Scarlata, C., Grogin, N.A., Conselice, C.J., Dahlen, T., Lotz, J.M., Dickinson, M., Lin, L.: The Relative Abundance of Compact and Normal Massive Early-type Galaxies and Its Evolution from Redshift z ~2 to the Present. Astrophys. J. **743**(1), 96 (2011) https://doi.org/10.1088/0004-637X/743/1/96 arXiv:1106.4308 [astro-ph.CO]

[20] Cassata, P., Giavalisco, M., Williams, C.C., Guo, Y., Lee, B., Renzini, A., Ferguson, H., Faber, S.F., Barro, G., McIntosh, D.H., Lu, Y., Bell, E.F., Koo, D.C., Papovich, C.J., Ryan, R.E., Conselice, C.J., Grogin, N., Koekemoer, A., Hathi, N.P.: Constraining the Assembly of Normal and Compact Passively Evolving Galaxies from Redshift z = 3 to the Present with CANDELS. Astrophys. J. **775**(2), 106 (2013) https://doi.org/10.1088/0004-637X/775/2/106 arXiv:1303.2689 [astro-ph.CO]

[21] Wright, L., Whitaker, K.E., Weaver, J.R., Cutler, S.E., Wang, B., Carnall, A., Suess, K.A., Bezanson, R., Nelson, E., Miller, T.B., Ito, K., Valentino, F.: Remarkably Compact Quiescent Candidates at 3 < z < 5 in JWST-CEERS. arXiv e-prints, 2311–05394 (2023) https://doi.org/10.48550/arXiv.2311.05394 arXiv:2311.05394 [astro-ph.GA]

[22] Szomoru, D., Franx, M., van Dokkum, P.G.: Sizes and Surface Brightness Profiles of Quiescent Galaxies at z ~2. Astrophys. J. **749**(2), 121 (2012) https://doi.org/10.1088/0004-637X/749/2/121 arXiv:1111.3361 [astro-ph.CO]

[23] Williams, C.C., Giavalisco, M., Cassata, P., Tundo, E., Wiklind, T., Guo, Y., Lee, B., Barro, G., Wuyts, S., Bell, E.F., Conselice, C.J., Dekel, A., Faber, S.M., Ferguson, H.C., Grogin, N., Hathi, N., Huang, K.-H., Kocevski, D., Koekemoer, A., Koo, D.C., Ravindranath, S., Salimbeni, S.: The Progenitors of the Compact Early-type Galaxies at High Redshift. Astrophys. J. **780**(1), 1 (2014) https://doi.org/10.1088/0004-637X/780/1/1 arXiv:1310.3819 [astro-ph.CO]

[24] Giavalisco, M., Ferguson, H.C., Koekemoer, A.M., Dickinson, M., Alexander, D.M., Bauer, F.E., Bergeron, J., Biagetti, C., Brandt, W.N., Casertano, S.,

Cesarsky, C., Chatzichristou, E., Conselice, C., Cristiani, S., Da Costa, L., Dahlen, T., de Mello, D., Eisenhardt, P., Erben, T., Fall, S.M., Fassnacht, C., Fosbury, R., Fruchter, A., Gardner, J.P., Grogin, N., Hook, R.N., Hornschemeier, A.E., Idzi, R., Jogee, S., Kretchmer, C., Laidler, V., Lee, K.S., Livio, M., Lucas, R., Madau, P., Mobasher, B., Moustakas, L.A., Nonino, M., Padovani, P., Papovich, C., Park, Y., Ravindranath, S., Renzini, A., Richardson, M., Riess, A., Rosati, P., Schirmer, M., Schreier, E., Somerville, R.S., Spinrad, H., Stern, D., Stiavelli, M., Strolger, L., Urry, C.M., Vandame, B., Williams, R., Wolf, C.: The Great Observatories Origins Deep Survey: Initial Results from Optical and Near-Infrared Imaging. Astrophys. J. **600**(2), 93–98 (2004) https://doi.org/10.1086/379232 arXiv:astro-ph/0309105 [astro-ph]

[25] Eisenstein, D.J., Willott, C., Alberts, S., Arribas, S., Bonaventura, N., Bunker, A.J., Cameron, A.J., Carniani, S., Charlot, S., Curtis-Lake, E., D'Eugenio, F., Endsley, R., Ferruit, P., Giardino, G., Hainline, K., Hausen, R., Jakobsen, P., Johnson, B.D., Maiolino, R., Rieke, M., Rieke, G., Rix, H.-W., Robertson, B., Stark, D.P., Tacchella, S., Williams, C.C., Willmer, C.N.A., Baker, W.M., Baum, S., Bhatawdekar, R., Boyett, K., Chen, Z., Chevallard, J., Circosta, C., Curti, M., Danhaive, A.L., DeCoursey, C., de Graaff, A., Dressler, A., Egami, E., Helton, J.M., Hviding, R.E., Ji, Z., Jones, G.C., Kumari, N., Lützgendorf, N., Laseter, I., Looser, T.J., Lyu, J., Maseda, M.V., Nelson, E., Parlanti, E., Perna, M., Puskás, D., Rawle, T., Rodríguez Del Pino, B., Sandles, L., Saxena, A., Scholtz, J., Sharpe, K., Shivaei, I., Silcock, M.S., Simmonds, C., Skarbinski, M., Smit, R., Stone, M., Suess, K.A., Sun, F., Tang, M., Topping, M.W., Übler, H., Villanueva, N.C., Wallace, I.E.B., Whitler, L., Witstok, J., Woodrum, C.: Overview of the JWST Advanced Deep Extragalactic Survey (JADES). arXiv e-prints, 2306–02465 (2023) https://doi.org/10.48550/arXiv.2306.02465 arXiv:2306.02465 [astro-ph.GA]

[26] Williams, C.C., Tacchella, S., Maseda, M.V., Robertson, B.E., Johnson, B.D., Willott, C.J., Eisenstein, D.J., Willmer, C.N.A., Ji, Z., Hainline, K.N., Helton, J.M., Alberts, S., Baum, S., Bhatawdekar, R., Boyett, K., Bunker, A.J., Carniani, S., Charlot, S., Chevallard, J., Curtis-Lake, E., de Graaff, A., Egami, E., Franx, M., Kumari, N., Maiolino, R., Nelson, E.J., Rieke, M.J., Sandles, L., Shivaei, I., Simmonds, C., Smit, R., Suess, K.A., Sun, F., Übler, H., Witstok, J.: JEMS: A Deep Medium-band Imaging Survey in the Hubble Ultra Deep Field with JWST NIRCam and NIRISS. ApJS **268**(2), 64 (2023) https://doi.org/10.3847/1538-4365/acf130 arXiv:2301.09780 [astro-ph.GA]

[27] Draine, B.T., Li, A.: Infrared Emission from Interstellar Dust. IV. The Silicate-Graphite-PAH Model in the Post-Spitzer Era. Astrophys. J. **657**(2), 810–837 (2007) https://doi.org/10.1086/511055 arXiv:astro-ph/0608003 [astro-ph]

[28] Rieke, G.H., Alonso-Herrero, A., Weiner, B.J., Pérez-González, P.G., Blaylock, M., Donley, J.L., Marcillac, D.: Determining Star Formation Rates for Infrared Galaxies. Astrophys. J. **692**(1), 556–573 (2009) https://doi.org/10.1088/

0004-637X/692/1/556 arXiv:0810.4150 [astro-ph]

[29] Lyu, J., Rieke, G.H., Alberts, S.: The Contribution of Host Galaxies to the Infrared Energy Output of z $\gtrsim$ 5.0 Quasars. Astrophys. J. **816**(2), 85 (2016) https://doi.org/10.3847/0004-637X/816/2/85 arXiv:1511.05938 [astro-ph.GA]

[30] Koshida, S., Minezaki, T., Yoshii, Y., Kobayashi, Y., Sakata, Y., Sugawara, S., Enya, K., Suganuma, M., Tomita, H., Aoki, T., Peterson, B.A.: Reverberation Measurements of the Inner Radius of the Dust Torus in 17 Seyfert Galaxies. Astrophys. J. **788**(2), 159 (2014) https://doi.org/10.1088/0004-637X/788/2/159 arXiv:1406.2078 [astro-ph.GA]

[31] Lyu, J., Rieke, G.H., Smith, P.S.: Mid-IR Variability and Dust Reverberation Mapping of Low-z Quasars. I. Data, Methods, and Basic Results. Astrophys. J. **886**(1), 33 (2019) https://doi.org/10.3847/1538-4357/ab481d arXiv:1909.11101 [astro-ph.GA]

[32] Casey, C.M., Cooray, A., Killi, M., Capak, P., Chen, C.-C., Hung, C.-L., Kartaltepe, J., Sanders, D.B., Scoville, N.Z.: Near-infrared MOSFIRE Spectra of Dusty Star-forming Galaxies at 0.2 ¡ z ¡ 4. Astrophys. J. **840**(2), 101 (2017) https://doi.org/10.3847/1538-4357/aa6cb1 arXiv:1703.10168 [astro-ph.GA]

[33] Hatsukade, B., Kohno, K., Yamaguchi, Y., Umehata, H., Ao, Y., Aretxaga, I., Caputi, K.I., Dunlop, J.S., Egami, E., Espada, D., Fujimoto, S., Hayatsu, N.H., Hughes, D.H., Ikarashi, S., Iono, D., Ivison, R.J., Kawabe, R., Kodama, T., Lee, M., Matsuda, Y., Nakanishi, K., Ohta, K., Ouchi, M., Rujopakarn, W., Suzuki, T., Tamura, Y., Ueda, Y., Wang, T., Wang, W.-H., Wilson, G.W., Yoshimura, Y., Yun, M.S.: ALMA twenty-six arcmin^2 survey of GOODS-S at one millimeter (ASAGAO): Source catalog and number counts. PASJ **70**(6), 105 (2018) https://doi.org/10.1093/pasj/psy104 arXiv:1808.04502 [astro-ph.GA]

[34] Williams, C.C., Alberts, S., Ji, Z., Hainline, K.N., Lyu, J., Rieke, G., Endsley, R., Suess, K.A., Sun, F., Johnson, B.D., Florian, M., Shivaei, I., Rujopakarn, W., Baker, W.M., Bhatawdekar, R., Boyett, K., Bunker, A.J., Cameron, A.J., Carniani, S., Charlot, S., Curtis-Lake, E., DeCoursey, C., de Graaff, A., Egami, E., Eisenstein, D.J., Gibson, J.L., Hausen, R., Helton, J.M., Maiolino, R., Maseda, M.V., Nelson, E.J., Pérez-González, P.G., Rieke, M.J., Robertson, B.E., Saxena, A., Tacchella, S., Willmer, C.N.A., Willott, C.J.: The Galaxies Missed by Hubble and ALMA: The Contribution of Extremely Red Galaxies to the Cosmic Census at 3 ¡ z ¡ 8. Astrophys. J. **968**(1), 34 (2024) https://doi.org/10.3847/1538-4357/ad3f17 arXiv:2311.07483 [astro-ph.GA]

[35] De Rossi, M.E., Rieke, G.H., Shivaei, I., Bromm, V., Lyu, J.: The Far-infrared Emission of the First Massive Galaxies. Astrophys. J. **869**(1), 4 (2018) https://doi.org/10.3847/1538-4357/aaebf8 arXiv:1810.10130 [astro-ph.GA]

29

[36] Dekel, A., Burkert, A.: Wet disc contraction to galactic blue nuggets and quenching to red nuggets. Mon. Not. R. Astron. Soc. **438**(2), 1870–1879 (2014) https://doi.org/10.1093/mnras/stt2331 arXiv:1310.1074 [astro-ph.CO]

[37] Danovich, M., Dekel, A., Hahn, O., Ceverino, D., Primack, J.: Four phases of angular-momentum buildup in high-z galaxies: from cosmic-web streams through an extended ring to disc and bulge. Mon. Not. R. Astron. Soc. **449**(2), 2087–2111 (2015) https://doi.org/10.1093/mnras/stv270 arXiv:1407.7129 [astro-ph.GA]

[38] Tacchella, S., Dekel, A., Carollo, C.M., Ceverino, D., DeGraf, C., Lapiner, S., Mandelker, N., Primack Joel, R.: The confinement of star-forming galaxies into a main sequence through episodes of gas compaction, depletion and replenishment. Mon. Not. R. Astron. Soc. **457**(3), 2790–2813 (2016) https://doi.org/10.1093/mnras/stw131 arXiv:1509.02529 [astro-ph.GA]

[39] Dekel, A., Lapiner, S., Ginzburg, O., Freundlich, J., Jiang, F., Finish, B., Kretschmer, M., Lin, D., Ceverino, D., Primack, J., Giavalisco, M., Ji, Z.: Origin of star-forming rings around massive centres in massive galaxies at z ¡ 4. Mon. Not. R. Astron. Soc. **496**(4), 5372–5398 (2020) https://doi.org/10.1093/mnras/staa1713 arXiv:2003.08984 [astro-ph.GA]

[40] Lapiner, S., Dekel, A., Freundlich, J., Ginzburg, O., Jiang, F., Kretschmer, M., Tacchella, S., Ceverino, D., Primack, J.: Wet compaction to a blue nugget: a critical phase in galaxy evolution. Mon. Not. R. Astron. Soc. **522**(3), 4515–4547 (2023) https://doi.org/10.1093/mnras/stad1263 arXiv:2302.12234 [astro-ph.GA]

[41] Lapiner, S., Dekel, A., Dubois, Y.: Compaction-driven black hole growth. Mon. Not. R. Astron. Soc. **505**(1), 172–190 (2021) https://doi.org/10.1093/mnras/stab1205 arXiv:2012.09186 [astro-ph.GA]

[42] Byrne, L., Faucher-Giguère, C.-A., Stern, J., Anglés-Alcázar, D., Wellons, S., Gurvich, A.B., Hopkins, P.F.: Stellar feedback-regulated black hole growth: driving factors from nuclear to halo scales. Mon. Not. R. Astron. Soc. **520**(1), 722–739 (2023) https://doi.org/10.1093/mnras/stad171 arXiv:2210.09320 [astro-ph.GA]

[43] Pathak, D., Belli, S., Weinberger, R.: Quenching, Mergers, and Age Profiles for z = 2 Galaxies in IllustrisTNG. Astrophys. J. **916**(2), 23 (2021) https://doi.org/10.3847/2041-8213/ac13a7 arXiv:2105.02234 [astro-ph.GA]

[44] Hartley, A.I., Nelson, E.J., Suess, K.A., Garcia, A.M., Park, M., Hernquist, L., Bezanson, R., Nevin, R., Pillepich, A., Schechter, A.L., Terrazas, B.A., Torrey, P., Wellons, S., Whitaker, K.E., Williams, C.C.: The first quiescent galaxies in TNG300. Mon. Not. R. Astron. Soc. **522**(2), 3138–3144 (2023) https://doi.org/10.1093/mnras/stad1162 arXiv:2304.09392 [astro-ph.GA]

[45] Park, M., Belli, S., Conroy, C., Tacchella, S., Leja, J., Cutler, S.E., Johnson, B.D., Nelson, E.J., Emami, R.: Rapid Quenching of Galaxies at Cosmic Noon.

Astrophys. J. **953**(1), 119 (2023) https://doi.org/10.3847/1538-4357/acd54a arXiv:2210.03747 [astro-ph.GA]

[46] Kurinchi-Vendhan, S., Farcy, M., Hirschmann, M., Valentino, F.: On the origin of star-formation quenching in massive galaxies at $zrsim3$ in the cosmological simulations IllustrisTNG. arXiv e-prints, 2310–03083 (2023) https://doi.org/10.48550/arXiv.2310.03083 arXiv:2310.03083 [astro-ph.GA]

[47] Kimmig, L.C., Remus, R.-S., Seidel, B., Valenzuela, L.M., Dolag, K., Burkert, A.: Blowing out the Candle: How to Quench Galaxies at High Redshift – an Ensemble of Rapid Starbursts, AGN Feedback and Environment. arXiv e-prints, 2310–16085 (2023) https://doi.org/10.48550/arXiv.2310.16085 arXiv:2310.16085 [astro-ph.GA]

[48] Maiolino, R., Scholtz, J., Curtis-Lake, E., Carniani, S., Baker, W., de Graaff, A., Tacchella, S., Übler, H., D'Eugenio, F., Witstok, J., Curti, M., Arribas, S., Bunker, A.J., Charlot, S., Chevallard, J., Eisenstein, D.J., Egami, E., Ji, Z., Jones, G.C., Lyu, J., Rawle, T., Robertson, B., Rujopakarn, W., Perna, M., Sun, F., Venturi, G., Williams, C.C., Willott, C.: JADES. The diverse population of infant Black Holes at 4¡z¡11: merging, tiny, poor, but mighty. arXiv e-prints, 2308–01230 (2023) https://doi.org/10.48550/arXiv.2308.01230 arXiv:2308.01230 [astro-ph.GA]

[49] Stone, M.A., Lyu, J., Rieke, G.H., Alberts, S., Hainline, K.N.: Undermassive Host Galaxies of Five $z \sim 6$ Luminous Quasars Detected with JWST. Astrophys. J. **964**(1), 90 (2024) https://doi.org/10.3847/1538-4357/ad2a57 arXiv:2310.18395 [astro-ph.GA]

[50] Eisenstein, D.J., Johnson, B.D., Robertson, B., Tacchella, S., Hainline, K., Jakobsen, P., Maiolino, R., Bonaventura, N., Bunker, A.J., Cameron, A.J., Cargile, P.A., Curtis-Lake, E., Hausen, R., Puskás, D., Rieke, M., Sun, F., Willmer, C.N.A., Willott, C., Alberts, S., Arribas, S., Baker, W.M., Baum, S., Bhatawdekar, R., Carniani, S., Charlot, S., Chen, Z., Chevallard, J., Curti, M., DeCoursey, C., D'Eugenio, F., de Graaff, A., Egami, E., Helton, J.M., Ji, Z., Jones, G.C., Kumari, N., Lützgendorf, N., Laseter, I., Looser, T.J., Lyu, J., Maseda, M.V., Nelson, E., Parlanti, E., Rauscher, B.J., Rawle, T., Rieke, G., Rix, H.-W., Rujopakarn, W., Sandles, L., Saxena, A., Scholtz, J., Sharpe, K., Shivaei, I., Simmonds, C., Smit, R., Topping, M.W., Übler, H., Venturi, G., Williams, C.C., Witstok, J., Woodrum, C.: The JADES Origins Field: A New JWST Deep Field in the JADES Second NIRCam Data Release. arXiv e-prints, 2310–12340 (2023) https://doi.org/10.48550/arXiv.2310.12340 arXiv:2310.12340 [astro-ph.GA]

[51] Oesch, P.A., Brammer, G., Naidu, R.P., Bouwens, R.J., Chisholm, J., Illingworth, G.D., Matthee, J., Nelson, E., Qin, Y., Reddy, N., Shapley, A., Shivaei, I., van Dokkum, P., Weibel, A., Whitaker, K., Wuyts, S., Covelo-Paz, A., Endsley, R.,

Fudamoto, Y., Giovinazzo, E., Herard-Demanche, T., Kerutt, J., Kramarenko, I., Labbe, I., Leonova, E., Lin, J., Magee, D., Marchesini, D., Maseda, M., Mason, C., Matharu, J., Meyer, R.A., Neufeld, C., Prieto Lyon, G., Schaerer, D., Sharma, R., Shuntov, M., Smit, R., Stefanon, M., Wyithe, J.S.B., Xiao, M.: The JWST FRESCO survey: legacy NIRCam/grism spectroscopy and imaging in the two GOODS fields. Mon. Not. R. Astron. Soc. **525**(2), 2864–2874 (2023) https://doi.org/10.1093/mnras/stad2411 arXiv:2304.02026 [astro-ph.GA]

[52] Rieke, M.J., Robertson, B., Tacchella, S., Hainline, K., Johnson, B.D., Hausen, R., Ji, Z., Willmer, C.N.A., Eisenstein, D.J., Puskás, D., Alberts, S., Arribas, S., Baker, W.M., Baum, S., Bhatawdekar, R., Bonaventura, N., Boyett, K., Bunker, A.J., Cameron, A.J., Carniani, S., Charlot, S., Chevallard, J., Chen, Z., Curti, M., Curtis-Lake, E., Danhaive, A.L., DeCoursey, C., Dressler, A., Egami, E., Endsley, R., Helton, J.M., Hviding, R.E., Kumari, N., Looser, T.J., Lyu, J., Maiolino, R., Maseda, M.V., Nelson, E.J., Rieke, G., Rix, H.-W., Sandles, L., Saxena, A., Sharpe, K., Shivaei, I., Skarbinski, M., Smit, R., Stark, D.P., Stone, M., Suess, K.A., Sun, F., Topping, M., Übler, H., Villanueva, N.C., Wallace, I.E.B., Williams, C.C., Willott, C., Whitler, L., Witstok, J., Woodrum, C.: JADES Initial Data Release for the Hubble Ultra Deep Field: Revealing the Faint Infrared Sky with Deep JWST NIRCam Imaging. ApJS **269**(1), 16 (2023) https://doi.org/10.3847/1538-4365/acf44d arXiv:2306.02466 [astro-ph.GA]

[53] Gaia Collaboration, Brown, A.G.A., Vallenari, A., Prusti, T., de Bruijne, J.H.J., Babusiaux, C., Biermann, M., Creevey, O.L., Evans, D.W., Eyer, L., Hutton, A., Jansen, F., Jordi, C., Klioner, S.A., Lammers, U., Lindegren, L., Luri, X., Mignard, F., Panem, C., Pourbaix, D., Randich, S., Sartoretti, P., Soubiran, C., Walton, N.A., Arenou, F., Bailer-Jones, C.A.L., Bastian, U., Cropper, M., Drimmel, R., Katz, D., Lattanzi, M.G., van Leeuwen, F., Bakker, J., Cacciari, C., Castañeda, J., De Angeli, F., Ducourant, C., Fabricius, C., Fouesneau, M., Frémat, Y., Guerra, R., Guerrier, A., Guiraud, J., Jean-Antoine Piccolo, A., Masana, E., Messineo, R., Mowlavi, N., Nicolas, C., Nienartowicz, K., Pailler, F., Panuzzo, P., Riclet, F., Roux, W., Seabroke, G.M., Sordo, R., Tanga, P., Thévenin, F., Gracia-Abril, G., Portell, J., Teyssier, D., Altmann, M., Andrae, R., Bellas-Velidis, I., Benson, K., Berthier, J., Blomme, R., Brugaletta, E., Burgess, P.W., Busso, G., Carry, B., Cellino, A., Cheek, N., Clementini, G., Damerdji, Y., Davidson, M., Delchambre, L., Dell'Oro, A., Fernández-Hernández, J., Galluccio, L., García-Lario, P., Garcia-Reinaldos, M., González-Núñez, J., Gosset, E., Haigron, R., Halbwachs, J.-L., Hambly, N.C., Harrison, D.L., Hatzidimitriou, D., Heiter, U., Hernández, J., Hestroffer, D., Hodgkin, S.T., Holl, B., Janßen, K., Jevardat de Fombelle, G., Jordan, S., Krone-Martins, A., Lanzafame, A.C., Löffler, W., Lorca, A., Manteiga, M., Marchal, O., Marrese, P.M., Moitinho, A., Mora, A., Muinonen, K., Osborne, P., Pancino, E., Pauwels, T., Petit, J.-M., Recio-Blanco, A., Richards, P.J., Riello, M., Rimoldini, L., Robin, A.C., Roegiers, T., Rybizki, J., Sarro, L.M., Siopis, C., Smith, M., Sozzetti, A., Ulla, A., Utrilla, E., van Leeuwen, M., van Reeven, W., Abbas, U., Abreu Aramburu, A., Accart, S., Aerts, C., Aguado, J.J., Ajaj, M., Altavilla, G., Álvarez, M.A.,

Álvarez Cid-Fuentes, J., Alves, J., Anderson, R.I., Anglada Varela, E., Antoja, T., Audard, M., Baines, D., Baker, S.G., Balaguer-Núñez, L., Balbinot, E., Balog, Z., Barache, C., Barbato, D., Barros, M., Barstow, M.A., Bartolomé, S., Bassilana, J.-L., Bauchet, N., Baudesson-Stella, A., Becciani, U., Bellazzini, M., Bernet, M., Bertone, S., Bianchi, L., Blanco-Cuaresma, S., Boch, T., Bombrun, A., Bossini, D., Bouquillon, S., Bragaglia, A., Bramante, L., Breedt, E., Bressan, A., Brouillet, N., Bucciarelli, B., Burlacu, A., Busonero, D., Butkevich, A.G., Buzzi, R., Caffau, E., Cancelliere, R., Cánovas, H., Cantat-Gaudin, T., Carballo, R., Carlucci, T., Carnerero, M.I., Carrasco, J.M., Casamiquela, L., Castellani, M., Castro-Ginard, A., Castro Sampol, P., Chaoul, L., Charlot, P., Chemin, L., Chiavassa, A., Cioni, M.-R.L., Comoretto, G., Cooper, W.J., Cornez, T., Cowell, S., Crifo, F., Crosta, M., Crowley, C., Dafonte, C., Dapergolas, A., David, M., David, P., de Laverny, P., De Luise, F., De March, R., De Ridder, J., de Souza, R., de Teodoro, P., de Torres, A., del Peloso, E.F., del Pozo, E., Delbo, M., Delgado, A., Delgado, H.E., Delisle, J.-B., Di Matteo, P., Diakite, S., Diener, C., Distefano, E., Dolding, C., Eappachen, D., Edvardsson, B., Enke, H., Esquej, P., Fabre, C., Fabrizio, M., Faigler, S., Fedorets, G., Fernique, P., Fienga, A., Figueras, F., Fouron, C., Fragkoudi, F., Fraile, E., Franke, F., Gai, M., Garabato, D., Garcia-Gutierrez, A., García-Torres, M., Garofalo, A., Gavras, P., Gerlach, E., Geyer, R., Giacobbe, P., Gilmore, G., Girona, S., Giuffrida, G., Gomel, R., Gomez, A., Gonzalez-Santamaria, I., González-Vidal, J.J., Granvik, M., Gutiérrez-Sánchez, R., Guy, L.P., Hauser, M., Haywood, M., Helmi, A., Hidalgo, S.L., Hilger, T., Hładczuk, N., Hobbs, D., Holland, G., Huckle, H.E., Jasniewicz, G., Jonker, P.G., Juaristi Campillo, J., Julbe, F., Karbevska, L., Kervella, P., Khanna, S., Kochoska, A., Kontizas, M., Kordopatis, G., Korn, A.J., Kostrzewa-Rutkowska, Z., Kruszyńska, K., Lambert, S., Lanza, A.F., Lasne, Y., Le Campion, J.-F., Le Fustec, Y., Lebreton, Y., Lebzelter, T., Leccia, S., Leclerc, N., Lecoeur-Taibi, I., Liao, S., Licata, E., Lindstrøm, E.P., Lister, T.A., Livanou, E., Lobel, A., Madrero Pardo, P., Managau, S., Mann, R.G., Marchant, J.M., Marconi, M., Marcos Santos, M.M.S., Marinoni, S., Marocco, F., Marshall, D.J., Martin Polo, L., Martín-Fleitas, J.M., Masip, A., Massari, D., Mastrobuono-Battisti, A., Mazeh, T., McMillan, P.J., Messina, S., Michalik, D., Millar, N.R., Mints, A., Molina, D., Molinaro, R., Molnár, L., Montegriffo, P., Mor, R., Morbidelli, R., Morel, T., Morris, D., Mulone, A.F., Munoz, D., Muraveva, T., Murphy, C.P., Musella, I., Noval, L., Ordénovic, C., Orrù, G., Osinde, J., Pagani, C., Pagano, I., Palaversa, L., Palicio, P.A., Panahi, A., Pawlak, M., Peñalosa Esteller, X., Penttilä, A., Piersimoni, A.M., Pineau, F.-X., Plachy, E., Plum, G., Poggio, E., Poretti, E., Poujoulet, E., Prša, A., Pulone, L., Racero, E., Ragaini, S., Rainer, M., Raiteri, C.M., Rambaux, N., Ramos, P., Ramos-Lerate, M., Re Fiorentin, P., Regibo, S., Reylé, C., Ripepi, V., Riva, A., Rixon, G., Robichon, N., Robin, C., Roelens, M., Rohrbasser, L., Romero-Gómez, M., Rowell, N., Royer, F., Rybicki, K.A., Sadowski, G., Sagristà Sellés, A., Sahlmann, J., Salgado, J., Salguero, E., Samaras, N., Sanchez Gimenez, V., Sanna, N., Santoveña, R., Sarasso, M., Schultheis, M., Sciacca, E., Segol, M., Segovia, J.C., Ségransan, D., Semeux, D., Shahaf, S., Siddiqui, H.I., Siebert, A., Siltala, L., Slezak, E., Smart, R.L., Solano, E., Solitro,

F., Souami, D., Souchay, J., Spagna, A., Spoto, F., Steele, I.A., Steidelmüller, H., Stephenson, C.A., Süveges, M., Szabados, L., Szegedi-Elek, E., Taris, F., Tauran, G., Taylor, M.B., Teixeira, R., Thuillot, W., Tonello, N., Torra, F., Torra, J., Turon, C., Unger, N., Vaillant, M., van Dillen, E., Vanel, O., Vecchiato, A., Viala, Y., Vicente, D., Voutsinas, S., Weiler, M., Wevers, T., Wyrzykowski, Ł., Yoldas, A., Yvard, P., Zhao, H., Zorec, J., Zucker, S., Zurbach, C., Zwitter, T.: Gaia Early Data Release 3. Summary of the contents and survey properties. Astron. Astrophys. **649**, 1 (2021) https://doi.org/10.1051/0004-6361/202039657 arXiv:2012.01533 [astro-ph.GA]

[54] Häußler, B., Bamford, S.P., Vika, M., Rojas, A.L., Barden, M., Kelvin, L.S., Alpaslan, M., Robotham, A.S.G., Driver, S.P., Baldry, I.K., Brough, S., Hopkins, A.M., Liske, J., Nichol, R.C., Popescu, C.C., Tuffs, R.J.: MegaMorph - multiwavelength measurement of galaxy structure: complete Sérsic profile information from modern surveys. Mon. Not. R. Astron. Soc. **430**(1), 330–369 (2013) https://doi.org/10.1093/mnras/sts633 arXiv:1212.3332 [astro-ph.CO]

[55] Häußler, B., Vika, M., Bamford, S.P., Johnston, E.J., Brough, S., Casura, S., Holwerda, B.W., Kelvin, L.S., Popescu, C.: GALAPAGOS-2/GALFITM/GAMA - Multi-wavelength measurement of galaxy structure: Separating the properties of spheroid and disk components in modern surveys. Astron. Astrophys. **664**, 92 (2022) https://doi.org/10.1051/0004-6361/202142935 arXiv:2204.05907 [astro-ph.GA]

[56] Peng, C.Y., Ho, L.C., Impey, C.D., Rix, H.-W.: Detailed Decomposition of Galaxy Images. II. Beyond Axisymmetric Models. Astron. J. **139**(6), 2097–2129 (2010) https://doi.org/10.1088/0004-6256/139/6/2097 arXiv:0912.0731 [astro-ph.CO]

[57] Ji, Z., Williams, C.C., Tacchella, S., Suess, K.A., Baker, W.M., Alberts, S., Bunker, A.J., Johnson, B.D., Robertson, B., Sun, F., Eisenstein, D.J., Rieke, M., Maseda, M.V., Hainline, K., Hausen, R., Rieke, G., Willmer, C.N.A., Egami, E., Shivaei, I., Carniani, S., Charlot, S., Chevallard, J., Curtis-Lake, E., Looser, T.J., Maiolino, R., Willott, C., Chen, Z., Helton, J.M., Lyu, J., Nelson, E., Bhatawdekar, R., Boyett, K., Sandles, L.: JADES + JEMS: A Detailed Look at the Buildup of Central Stellar Cores and Suppression of Star Formation in Galaxies at Redshifts 3 ¡ z ¡ 4.5. arXiv e-prints, 2305–18518 (2023) https://doi.org/10.48550/arXiv.2305.18518 arXiv:2305.18518 [astro-ph.GA]

[58] Perrin, M.D., Sivaramakrishnan, A., Lajoie, C.-P., Elliott, E., Pueyo, L., Ravindranath, S., Albert, L.: Updated point spread function simulations for JWST with WebbPSF. In: Oschmann, J. Jacobus M., Clampin, M., Fazio, G.G., MacEwen, H.A. (eds.) Space Telescopes and Instrumentation 2014: Optical, Infrared, and Millimeter Wave. Society of Photo-Optical Instrumentation Engineers (SPIE) Conference Series, vol. 9143, p. 91433 (2014). https://doi.org/10.1117/12.2056689

[59] Gáspár, A., Rieke, G.H., Guillard, P., Dicken, D., Gastaud, R., Alberts, S., Morrison, J., Ressler, M.E., Argyriou, I., Glasse, A.: The Quantum Efficiency and Diffractive Image Artifacts of Si:As IBC mid-IR Detector Arrays at 5-10 μm: Implications for the JWST/MIRI Detectors. PASP **133**(1019), 014504 (2021) https://doi.org/10.1088/1538-3873/abcd04 arXiv:2011.11908 [astro-ph.IM]

[60] Anderson, J., Bedin, L.R.: An Empirical Pixel-Based Correction for Imperfect CTE. I. HST's Advanced Camera for Surveys. PASP **122**(895), 1035 (2010) https://doi.org/10.1086/656399 arXiv:1007.3987 [astro-ph.IM]

[61] Dimauro, P., Huertas-Company, M., Daddi, E., Pérez-González, P.G., Bernardi, M., Barro, G., Buitrago, F., Caro, F., Cattaneo, A., Dominguez-Sánchez, H., Faber, S.M., Häußler, B., Kocevski, D.D., Koekemoer, A.M., Koo, D.C., Lee, C.T., Mei, S., Margalef-Bentabol, B., Primack, J., Rodriguez-Puebla, A., Salvato, M., Shankar, F., Tuccillo, D.: A catalog of polychromatic bulge-disc decompositions of ∼17.600 galaxies in CANDELS. Mon. Not. R. Astron. Soc. **478**(4), 5410–5426 (2018) https://doi.org/10.1093/mnras/sty1379 arXiv:1803.10234 [astro-ph.GA]

[62] Nedkova, K.V., Häußler, B., Marchesini, D., Dimauro, P., Brammer, G., Eigenthaler, P., Feinstein, A.D., Ferguson, H.C., Huertas-Company, M., Johnston, E.J., Kado-Fong, E., Kartaltepe, J.S., Labbé, I., Lange-Vagle, D., Martis, N.S., McGrath, E.J., Muzzin, A., Oesch, P., Ordenes-Briceño, Y., Puzia, T., Shipley, H.V., Simmons, B.D., Skelton, R.E., Stefanon, M., van der Wel, A., Whitaker, K.E.: Extending the evolution of the stellar mass-size relation at z ≤ 2 to low stellar mass galaxies from HFF and CANDELS. Mon. Not. R. Astron. Soc. **506**(1), 928–956 (2021) https://doi.org/10.1093/mnras/stab1744 arXiv:2106.07663 [astro-ph.GA]

[63] van der Wel, A., Bell, E.F., Häussler, B., McGrath, E.J., Chang, Y.-Y., Guo, Y., McIntosh, D.H., Rix, H.-W., Barden, M., Cheung, E., Faber, S.M., Ferguson, H.C., Galametz, A., Grogin, N.A., Hartley, W., Kartaltepe, J.S., Kocevski, D.D., Koekemoer, A.M., Lotz, J., Mozena, M., Peth, M.A., Peng, C.Y.: Structural Parameters of Galaxies in CANDELS. ApJS **203**(2), 24 (2012) https://doi.org/10.1088/0067-0049/203/2/24 arXiv:1211.6954 [astro-ph.CO]

[64] Johnson, B.D., Leja, J., Conroy, C., Speagle, J.S.: Stellar Population Inference with Prospector. ApJS **254**(2), 22 (2021) https://doi.org/10.3847/1538-4365/abef67 arXiv:2012.01426 [astro-ph.GA]

[65] Kroupa, P.: On the variation of the initial mass function. Mon. Not. R. Astron. Soc. **322**(2), 231–246 (2001) https://doi.org/10.1046/j.1365-8711.2001.04022.x arXiv:astro-ph/0009005 [astro-ph]

[66] Conroy, C., Gunn, J.E., White, M.: The Propagation of Uncertainties in Stellar Population Synthesis Modeling. I. The Relevance of Uncertain Aspects of

Stellar Evolution and the Initial Mass Function to the Derived Physical Properties of Galaxies. Astrophys. J. **699**(1), 486–506 (2009) https://doi.org/10.1088/0004-637X/699/1/486 arXiv:0809.4261 [astro-ph]

[67] Conroy, C., Gunn, J.E.: The Propagation of Uncertainties in Stellar Population Synthesis Modeling. III. Model Calibration, Comparison, and Evaluation. Astrophys. J. **712**(2), 833–857 (2010) https://doi.org/10.1088/0004-637X/712/2/833 arXiv:0911.3151 [astro-ph.CO]

[68] Choi, J., Dotter, A., Conroy, C., Cantiello, M., Paxton, B., Johnson, B.D.: Mesa Isochrones and Stellar Tracks (MIST). I. Solar-scaled Models. Astrophys. J. **823**(2), 102 (2016) https://doi.org/10.3847/0004-637X/823/2/102 arXiv:1604.08592 [astro-ph.SR]

[69] Dotter, A.: MESA Isochrones and Stellar Tracks (MIST) 0: Methods for the Construction of Stellar Isochrones. ApJS **222**(1), 8 (2016) https://doi.org/10.3847/0067-0049/222/1/8 arXiv:1601.05144 [astro-ph.SR]

[70] Falcón-Barroso, J., Sánchez-Blázquez, P., Vazdekis, A., Ricciardelli, E., Cardiel, N., Cenarro, A.J., Gorgas, J., Peletier, R.F.: An updated MILES stellar library and stellar population models. Astron. Astrophys. **532**, 95 (2011) https://doi.org/10.1051/0004-6361/201116842 arXiv:1107.2303 [astro-ph.CO]

[71] Madau, P.: Radiative Transfer in a Clumpy Universe: The Colors of High-Redshift Galaxies. Astrophys. J. **441**, 18 (1995) https://doi.org/10.1086/175332

[72] Byler, N., Dalcanton, J.J., Conroy, C., Johnson, B.D.: Nebular Continuum and Line Emission in Stellar Population Synthesis Models. Astrophys. J. **840**(1), 44 (2017) https://doi.org/10.3847/1538-4357/aa6c66 arXiv:1611.08305 [astro-ph.GA]

[73] Charlot, S., Fall, S.M.: A Simple Model for the Absorption of Starlight by Dust in Galaxies. Astrophys. J. **539**(2), 718–731 (2000) https://doi.org/10.1086/309250 arXiv:astro-ph/0003128 [astro-ph]

[74] Noll, S., Burgarella, D., Giovannoli, E., Buat, V., Marcillac, D., Muñoz-Mateos, J.C.: Analysis of galaxy spectral energy distributions from far-UV to far-IR with CIGALE: studying a SINGS test sample. Astron. Astrophys. **507**(3), 1793–1813 (2009) https://doi.org/10.1051/0004-6361/200912497 arXiv:0909.5439 [astro-ph.CO]

[75] Calzetti, D., Armus, L., Bohlin, R.C., Kinney, A.L., Koornneef, J., Storchi-Bergmann, T.: The Dust Content and Opacity of Actively Star-forming Galaxies. Astrophys. J. **533**(2), 682–695 (2000) https://doi.org/10.1086/308692 arXiv:astro-ph/9911459 [astro-ph]

[76] Kriek, M., Conroy, C.: The Dust Attenuation Law in Distant Galaxies: Evidence

for Variation with Spectral Type. Astrophys. J. **775**(1), 16 (2013) https://doi.org/10.1088/2041-8205/775/1/L16 arXiv:1308.1099 [astro-ph.CO]

[77] Leja, J., Carnall, A.C., Johnson, B.D., Conroy, C., Speagle, J.S.: How to Measure Galaxy Star Formation Histories. II. Nonparametric Models. Astrophys. J. **876**(1), 3 (2019) https://doi.org/10.3847/1538-4357/ab133c arXiv:1811.03637 [astro-ph.GA]

[78] Tacchella, S., Conroy, C., Faber, S.M., Johnson, B.D., Leja, J., Barro, G., Cunningham, E.C., Deason, A.J., Guhathakurta, P., Guo, Y., Hernquist, L., Koo, D.C., McKinnon, K., Rockosi, C.M., Speagle, J.S., van Dokkum, P., Yesuf, H.M.: Fast, Slow, Early, Late: Quenching Massive Galaxies at z ∼ 0.8. Astrophys. J. **926**(2), 134 (2022) https://doi.org/10.3847/1538-4357/ac449b arXiv:2102.12494 [astro-ph.GA]

[79] Leja, J., Speagle, J.S., Ting, Y.-S., Johnson, B.D., Conroy, C., Whitaker, K.E., Nelson, E.J., van Dokkum, P., Franx, M.: A New Census of the 0.2 ¡ z ¡ 3.0 Universe. II. The Star-forming Sequence. Astrophys. J. **936**(2), 165 (2022) https://doi.org/10.3847/1538-4357/ac887d arXiv:2110.04314 [astro-ph.GA]

[80] Ji, Z., Giavalisco, M.: Reconstructing the Assembly of Massive Galaxies. I. The Importance of the Progenitor Effect in the Observed Properties of Quiescent Galaxies at z ≈ 2. Astrophys. J. **935**(2), 120 (2022) https://doi.org/10.3847/1538-4357/ac7f43 arXiv:2204.02414 [astro-ph.GA]

[81] Ji, Z., Giavalisco, M.: Reconstructing the Assembly of Massive Galaxies. II. Galaxies Develop Massive and Dense Stellar Cores as They Evolve and Head toward Quiescence at Cosmic Noon. Astrophys. J. **943**(1), 54 (2023) https://doi.org/10.3847/1538-4357/aca807 arXiv:2208.04325 [astro-ph.GA]

[82] Williams, C.C., Alberts, S., Ji, Z., Hainline, K.N., Lyu, J., Rieke, G., Endsley, R., Suess, K.A., Johnson, B.D., Florian, M., Shivaei, I., Rujopakarn, W., Baker, W.M., Bhatawdekar, R., Boyett, K., Bunker, A.J., Carniani, S., Charlot, S., Curtis-Lake, E., DeCoursey, C., de Graaff, A., Egami, E., Eisenstein, D.J., Gibson, J.L., Hausen, R., Helton, J.M., Maiolino, R., Maseda, M.V., Nelson, E.J., Perez-Gonzalez, P.G., Rieke, M.J., Robertson, B.E., Sun, F., Tacchella, S., Willmer, C.N.A., Willott, C.J.: The galaxies missed by Hubble and ALMA: the contribution of extremely red galaxies to the cosmic census at 3¡z¡8. arXiv e-prints, 2311–07483 (2023) https://doi.org/10.48550/arXiv.2311.07483 arXiv:2311.07483 [astro-ph.GA]

[83] Draine, B.T.: Interstellar Dust Grains. ARA&A **41**, 241–289 (2003) https://doi.org/10.1146/annurev.astro.41.011802.094840 arXiv:astro-ph/0304489 [astro-ph]

[84] Conroy, C.: Modeling the Panchromatic Spectral Energy Distributions of Galaxies. ARA&A **51**(1), 393–455 (2013) https://doi.org/10.1146/annurev-astro-082812-141017 arXiv:1301.7095 [astro-ph.CO]

[85] Nenkova, M., Sirocky, M.M., Ivezić, Ž., Elitzur, M.: AGN Dusty Tori. I. Handling of Clumpy Media. Astrophys. J. **685**(1), 147–159 (2008) https://doi.org/10.1086/590482 arXiv:0806.0511 [astro-ph]

[86] Nenkova, M., Sirocky, M.M., Nikutta, R., Ivezić, Ž., Elitzur, M.: AGN Dusty Tori. II. Observational Implications of Clumpiness. Astrophys. J. **685**(1), 160–180 (2008) https://doi.org/10.1086/590483 arXiv:0806.0512 [astro-ph]

[87] Carnall, A.C., McLeod, D.J., McLure, R.J., Dunlop, J.S., Begley, R., Cullen, F., Donnan, C.T., Hamadouche, M.L., Jewell, S.M., Jones, E.W., Pollock, C.L., Wild, V.: A surprising abundance of massive quiescent galaxies at 3 ¡ z ¡ 5 in the first data from JWST CEERS. Mon. Not. R. Astron. Soc. **520**(3), 3974–3985 (2023) https://doi.org/10.1093/mnras/stad369 arXiv:2208.00986 [astro-ph.GA]

[88] Lyu, J., Alberts, S., Rieke, G.H., Shivaei, I., Perez-Gonzalez, P.G., Sun, F., Hainline, K.N., Baum, S., Bonaventura, N., Bunker, A.J., Egami, E., Eisenstein, D.J., Florian, M., Ji, Z., Johnson, B.D., Morrison, J., Rieke, M., Robertson, B., Rujopakarn, W., Tacchella, S., Scholtz, J., Willmer, C.N.A.: AGN Selection and Demographics: A New Age with JWST/MIRI. arXiv e-prints, 2310–12330 (2023) https://doi.org/10.48550/arXiv.2310.12330 arXiv:2310.12330 [astro-ph.GA]

[89] Lyu, J., Alberts, S., Rieke, G.H., Rujopakarn, W.: AGN Selection and Demographics in GOODS-S/HUDF from X-Ray to Radio. Astrophys. J. **941**(2), 191 (2022) https://doi.org/10.3847/1538-4357/ac9e5d arXiv:2209.06219 [astro-ph.GA]

[90] Gordon, K.D., Clayton, G.C., Misselt, K.A., Landolt, A.U., Wolff, M.J.: A Quantitative Comparison of the Small Magellanic Cloud, Large Magellanic Cloud, and Milky Way Ultraviolet to Near-Infrared Extinction Curves. Astrophys. J. **594**(1), 279–293 (2003) https://doi.org/10.1086/376774 arXiv:astro-ph/0305257 [astro-ph]

[91] Greene, J.E., Ho, L.C.: Estimating Black Hole Masses in Active Galaxies Using the Hα Emission Line. Astrophys. J. **630**(1), 122–129 (2005) https://doi.org/10.1086/431897 arXiv:astro-ph/0508335 [astro-ph]

[92] Santini, P., Castellano, M., Merlin, E., Fontana, A., Fortuni, F., Kodra, D., Magnelli, B., Menci, N., Calabrò, A., Lovell, C.C., Pentericci, L., Testa, V., Wilkins, S.M.: The emergence of passive galaxies in the early Universe. Astron. Astrophys. **652**, 30 (2021) https://doi.org/10.1051/0004-6361/202039738 arXiv:2011.10584 [astro-ph.GA]

[93] Bruzual, G., Charlot, S.: Stellar population synthesis at the resolution of 2003. Mon. Not. R. Astron. Soc. **344**(4), 1000–1028 (2003) https://doi.org/10.1046/j.1365-8711.2003.06897.x arXiv:astro-ph/0309134 [astro-ph]

[94] Carnall, A.C., McLure, R.J., Dunlop, J.S., Davé, R.: Inferring the star formation

histories of massive quiescent galaxies with BAGPIPES: evidence for multiple quenching mechanisms. Mon. Not. R. Astron. Soc. **480**(4), 4379–4401 (2018) https://doi.org/10.1093/mnras/sty2169 arXiv:1712.04452 [astro-ph.GA]